

**Books/Book Chapters/Conference Papers 2017-18**

SI No.	Name of the Teacher	Title of the Paper/Books/Book Chapter	Title of the proceedings of the conference	Name of the conference	National/ International	Year of publication	ISBN/ISSN number of the proceeding	Affiliating Institute at the time of publication	Name of the Publisher
1	Garimella Raghu Chandra, K.V. Nagesha, and Vedala Rama Sastry	Image Processing Image Processing based Assessment of Blast Performance in Opencast Mines – Case Studies			International	19/01/2018	ISBN: 978-81-936117-0-8	Madanapalle Institute of Technology and Science	McGraw-Hill Education
2	Prof.K.Laxmipathi Rao	B.Sc Third year Physics (Solid State Physics)			National	2018	978-81-8180-543-0	Methodist college of Engineering and Technology	Telugu Academy
3	Akshay S K Naidu	Structural Health Monitoring Using Admittance Response of Piezoceramic Actuator Sensors	Proceedings of the 2nd International Conference on Innovations in Structural Engineering	Innovation in structural engineering -International conference	International	Dec/17		Methodist College of Engineering and Technology	
4	Shaista Begum, D. Rupesh Kumar, Sidra Khan	Study on mechanical properties of binary blended recycled aggregate concrete	Proceedings of the 2nd International Conference on Innovations in Structural Engineering	Innovation in structural engineering -International conference	International	29-31 DECEMBER2017		Deccan College of Engineering and Technology	
5	K.Shailaja	Progressive Genetic Evolutions-Based Join	Proceedings of the First International Conference on Computational Intelligence and Informatics, Advances in Intelligent Systems	ICCII	International	25-27, September, 2017 2017	978-981-10-2471-9	JNTUH	Springer
6	Dr.B.Krishna Kumar	Performance comparison of IST and Multi Scale Principal Component Analysis in the EEG signals	IEEE Conference, International Conference on Computing Methodologies and Communication	ICCMC	INTERNATIONAL	18-19 July 2017		MCET	IEEE CONFERENCE PROCEEDINGS

**PRINCIPAL**  
**METHODIST COLLEGE OF ENGG. & TECH.**  
 King Koti Road, Abids, Hyderabad



## Image Processing based Assessment of Blast Performance in Opencast Mines – Case Studies

<sup>1</sup>Garimella Raghu Chandra, <sup>2</sup>K.V. Nagesha and <sup>3</sup>Vedala Rama Sastry

<sup>1</sup>Department of Electrical and Electronics Engineering, Madanapalle Institute of Technology and Science, Angallu, Chittoor District, India. OCR ID: 0000-0003-3772-9965  
[raghuchandhra@india.com](mailto:raghuchandhra@india.com)

<sup>2</sup>Department of Mechanical Engineering, Madanapalle Institute of Technology and Science, Angallu, Chittoor District, India  
[kvnagesha@gmail.com](mailto:kvnagesha@gmail.com)

<sup>3</sup>Department of Mining Engineering, National Institute of Technology Karnataka, Surathkal, India

**Abstract.** Rock mass can be fractured by the process of blasting in which a known volume of the material is obtained by using a calculated quantity of explosive. Explosive selected for blasting will be depends on the factors like rock mass parameters, blasting economics, and blast design. Assessment of the performance of a given blast is essential in larger economics of mining project. A study was conducted to know the blast performance at two different mines located in Southern Part of India. High speed videography was used to assess the blast performance and wastage of gaseous energy. With increase in stemming height from 1.0m to 3.5m at different mines in earlier research, it was found that there will be decrease in the escape of gas ejection from 7.42m to 3.5m, which was almost half the height of ejection. Analysis made during the research shows that the maximum velocity of rock movement was found to be 8.97m/s in Mine-A and 12.40m/s in Mine-B. To determine the fragment size distribution, Wipfrag was used which gives quick and accurate measurements. Using Image Processing methodology, it was observed that Blast-4 of Mine-A with explosive charge of about 33.36kg/hole produced finer fragmentation compared to Blast-4 in Mine-B with same explosive charge.

**Keywords:** High speed videography; Rock mass movement; Fragmentation; Wipfrag.

p. 21-28

[Full article in PDF](#) |

---

© 2018 McGraw-Hill Education

ISBN: 978-81-936117-0-8

# Image Processing based Assessment of Blast Performance in Opencast Mines – Case Studies

Garimella Raghu Chandra\*, K.V. Nagesha\*\* and Vedala Rama Sastry\*\*\*

\*Department of Electrical and Electronics Engineering, Madanapalle Institute of Technology and Science, Angallu, Chittoor District, India

raghuchandhra@india.com, OCR ID: 0000-0003-3772-9965

\*\*Department of Mechanical Engineering, Madanapalle Institute of Technology and Science, Angallu, Chittoor District, India  
kvnagesha@gmail.com

\*\*\*Department of Mining Engineering, National Institute of Technology Karnataka, Surathkal, India

**Abstract:** Rock mass can be fractured by the process of blasting in which a known volume of the material is obtained by using a calculated quantity of explosive. Explosive selected for blasting will depend on the factors like rock mass parameters, blasting economics, and blast design. Assessment of the performance of a given blast is essential in larger economics of mining project. A study was conducted to know the blast performance at two different mines located in Southern Part of India. High speed videography was used to assess the blast performance and wastage of gaseous energy. With increase in stemming height from 1.0m to 3.5m at different mines in earlier research, it was found that there will be decrease in the escape of gas ejection from 7.42m to 3.5m, which was almost half the height of ejection. Analysis made during the research shows that the maximum velocity of rock movement was found to be 8.97m/s in Mine-A and 12.40m/s in Mine-B. To determine the fragment size distribution, Wipfrag was used which gives quick and accurate measurements. Using Image Processing methodology, it was observed that Blast-4 of Mine-A with explosive charge of about 33.36kg/hole produced finer fragmentation compared to Blast-4 in Mine-B with same explosive charge.

**Keywords:** High speed videography; Rock mass movement; Fragmentation; Wipfrag.

## Introduction

Rock blasting is done to break the rock mass into smaller pieces in mines and quarries. In order to achieve the desired objective to be performed in the field, precise engineering application of blasting operation is required. In civil engineering projects like construction of dams, tunnels or caverns hard rock mass has to be removed, using blasting process (Floyd, 1987; Nabiullah et al., 2002). Blasting process can be finished in few seconds and it is not possible to assess the performance of the blast with naked eye (Bhandari, 1997). To view the blast and analyse the design performance of a blast, high speed video camera is used, which can capture video and can be played back to view in slow motion (Chiappetta and Mammele, 1988). The paper aims at assessing the blast performance using High Speed Video Camera of AOS Technologies, Switzerland, in two different opencast limestone mines located in Southern India. Studies were carried out at limestone Mine-A of Tamilnadu State and limestone Mine-B of Andhra Pradesh State (Figure 1).

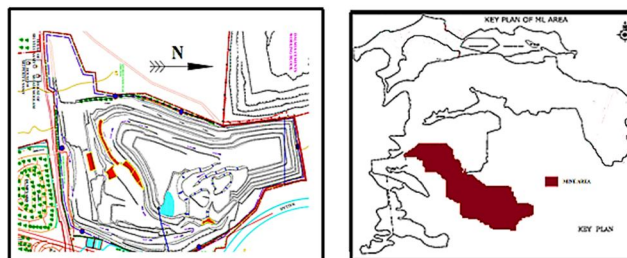


Figure 1a. Mine A

Figure 1b. Mine B

Figure 1. View of limestone mines

## Methodology

In total, 22 blasts were carried out in two mines to assess the performance of blasts using image processing technique. High speed video camera was used to record all the blasts (Figure 2). The parameters used in blasting studies are listed in Table 1.

Blastholes were of 115mm diameter in both mines A and B. Depth of blastholes was varying from 5m to 10m in Mine-A, 2m to 9.5m in Mine-B. The fragmentation in blasted muck piles was analysed by Wipfrag software. Slurry explosive available in the form of cartridges was used as primer and column charge in Mine-A, whereas in Mine-B slurry explosive available in the form of cartridges was used as primer and ANFO was used as column charge (CO, 1987).

Table 1. Summary of blasts studied

Limestone Mine-A					
Specifications	Blast Number				
	1	2	3	4	5
Bench height (m)	5.0	6.0	7.0	7.5	10.0
Burden (m)	2.5	2.5	2.5	2.5	2.5
Spacing (m)	3.0	3.0	3.0	3.0	3.0
No. of blastholes	13	24	23	18	20
Explosive/ hole (kg)	19.25	25.02	29.37	33.36	40.03
Total exp. charge (kg)	250.20	600.48	675.54	600.48	800.64
Stemming (m)	1.5	1.4	1.5	1.4	1.0

Limestone Mine-B					
Specifications	Blast Number				
	1	2	3	4	5
Bench height (m)	2.0	3.5	5.0	8.0	9.5
Burden (m)	2.0	2.0	3.0	2.5	3.0
Spacing (m)	3.0	3.0	5.0	5.0	6.0
No. of blastholes	17	12	10	27	15
Explosive/ hole (kg)	03.82	07.00	09.40	33.33	48.21
Total exp. charge (kg)	65.00	85.00	94.00	900.00	723.00
Stemming (m)	1.6	2.7	3.5	3.5	3.7

Image Processing Analysis obtained from the high speed videography of 1000 frames per second capacity was used to understand the dynamics involved in the blasts, which in turn reduce the costly trials that are necessary for optimizing the blast design. High speed video camera provides results on the spot and recorded video can be played using imaging studio (Chiappetta and Mammele, 1987; Sastry et al., 2015a).



Figure 2. High speed video camera of 1000fps capacity

Pro-analyst provides a series of video processing and motion analysis that can be applied to any video or image sequence which will allow users to measure the displacement and velocity of moving fragments (Sastry et al., 2014). It is also used to

track particles and know the ejection of gas energy from stemming zone of blasthole (Sastry et al., 2015b). Sequence of blasts with specific time intervals from the time of initiation in Mine-A and Mine-B was observed using high speed video camera and further image processing analysis was carried out using the recorded video (Figures 3 and 4).

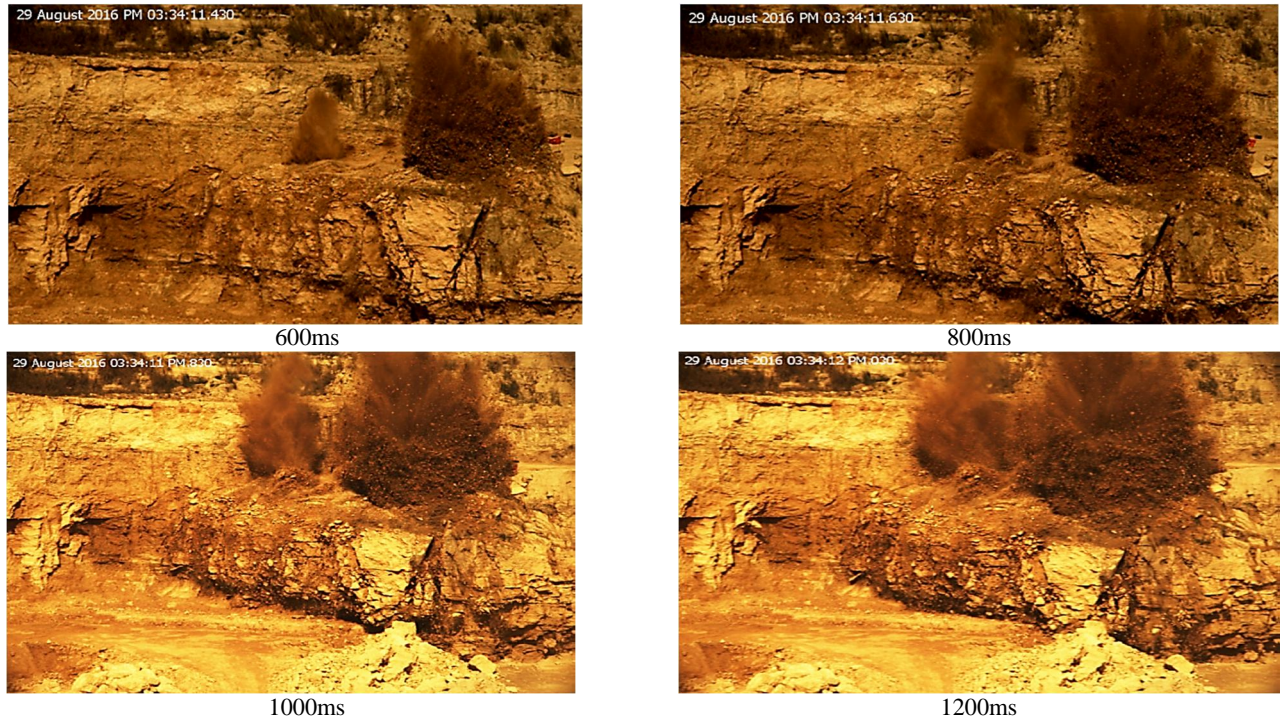


Figure 3. Typical blasting sequence in Mine-A

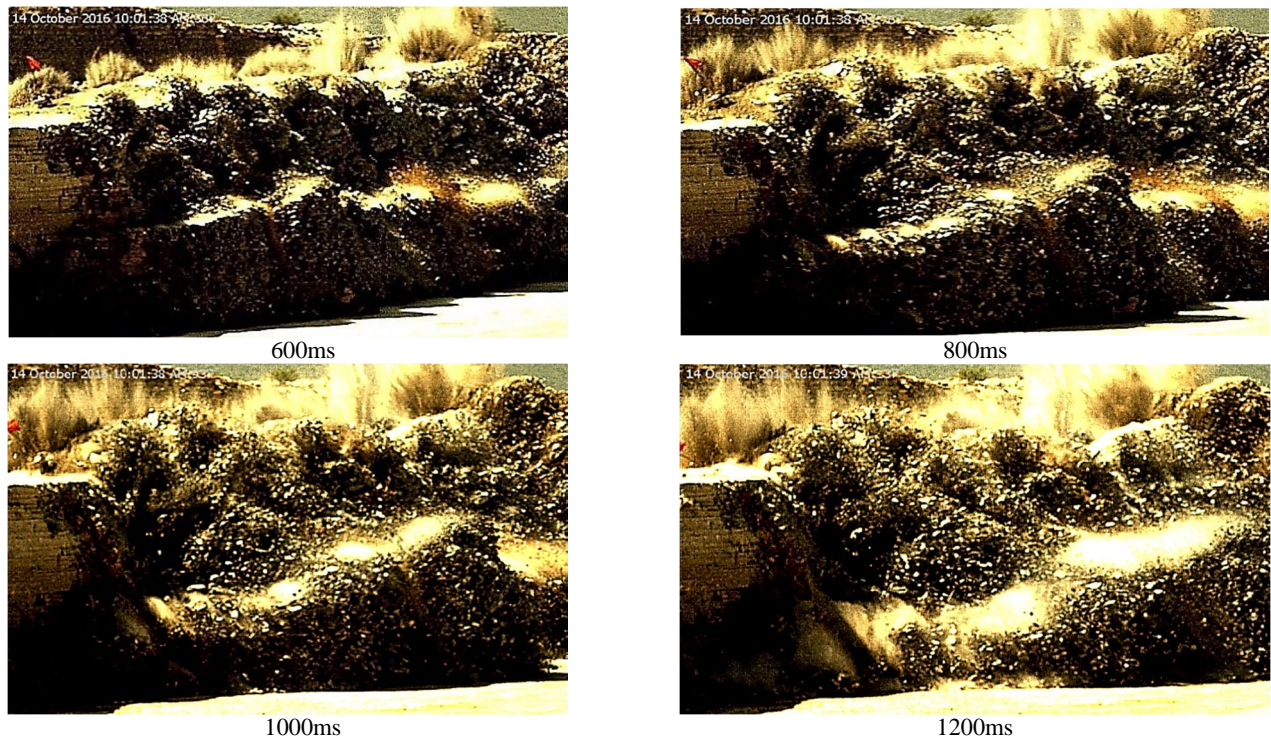


Figure 4. Typical blasting sequence in Mine-B

Fragmentation resulting from blasts was assessed by taking photos of muck pile generated from blasts. After each blast, photos were taken covering various layers of entire muck pile during the process of shovelling at regular intervals. Photos were collected and the process was continued till the entire muck pile got excavated. Wipfrag based image processing analysis was carried out to investigate the fragmentation. Wipfrag uses the technique of analysis of digital image processing of blasted rock to predict the grain size distribution in a muck pile. Scale device was used to view the reference of each sizing zone as a calibrator (Jha, 2013). Muck pile of a blast was photographed and image is then transferred to Wipfrag system. Muck pile generated from different production scale blasts are shown in Figure 5.



Figure 5. Typical muck pile obtained from the blasts

**Results and Discussion**

To track down the rock movement of bench face and find out the escape of gaseous energy, Pro-analyst was used (Ash, 1973). Research study based on image processing analysis revealed that the bench height of 10m in Mine-A resulted in gas ejection of 7.42m, whereas the bench height of 7.5m in the same mine resulted in gas ejection of 8.73m. Thus, it may be interpreted that wastage of gas energy was less in taller benches. Figure 6 shows typical case analysis in Mine-A, and Figure 7 for Mine-B.

Comparison of gas ejection from Mine-A and Mine-B using image processing results revealed that gas ejection was found to be more in Mine-A. This may be due to lesser stemming height in Mine-A when compared to Mine-B. Stemming height of 1.0m in Mine-A resulted in gas ejection of 7.42m, whereas stemming height of 3.5m in Mine-B which resulted in gas ejection of 3.82m, which was almost half the height in Mine-B.

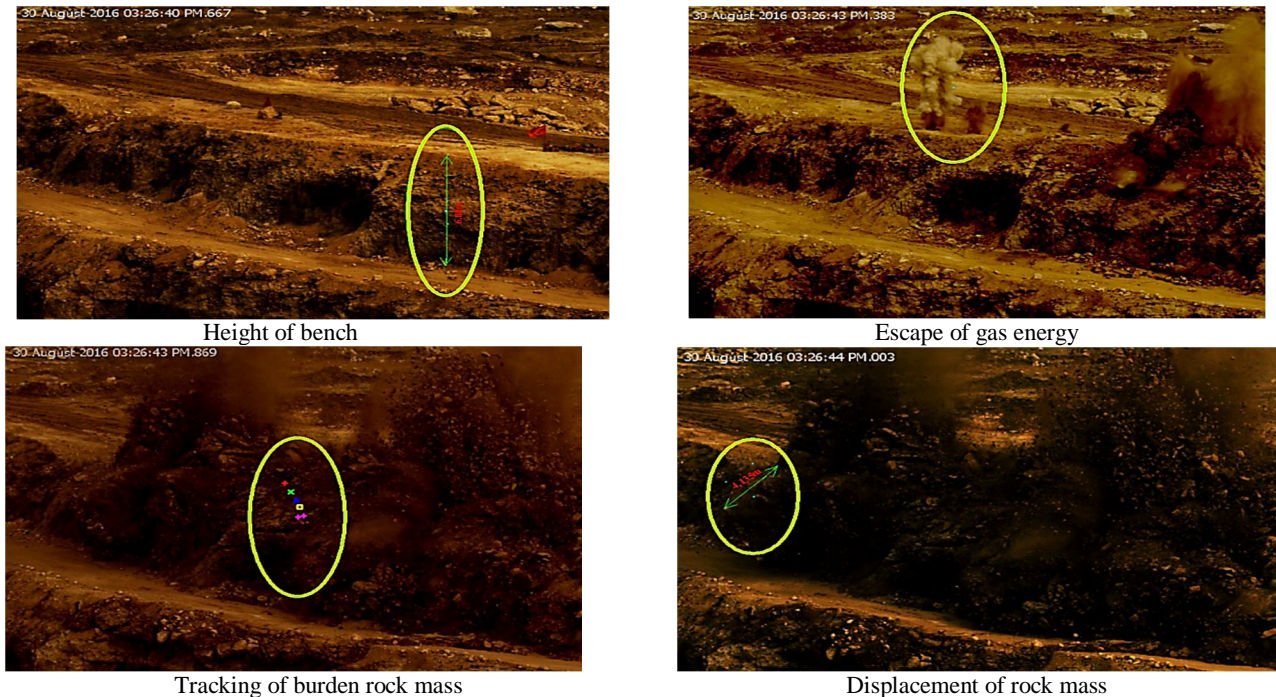


Figure 6. Analysis of a blast in Mine-A

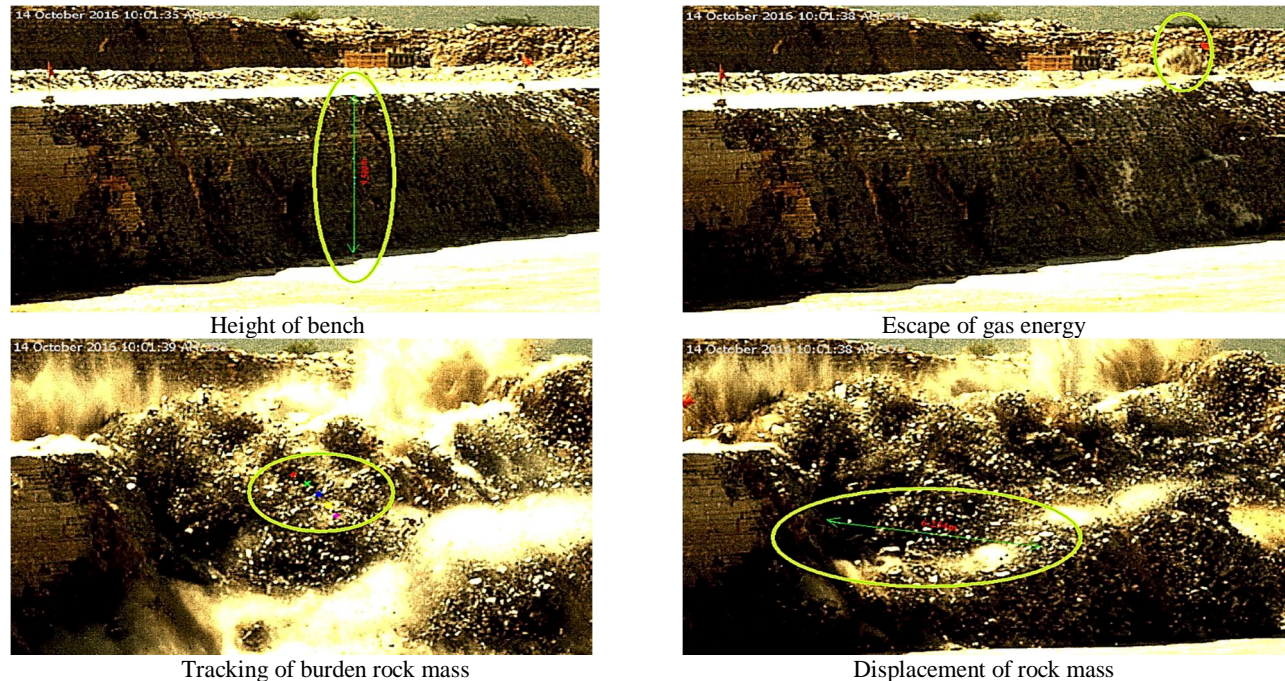


Figure 7. Analysis of a blast in Mine-B

Velocity of burden rock was varying from 6.58m/s to 8.97m/s in Mine-A and 8.34m/s to 12.4m/s in Mine-B. Burden rock movement was found to be greater in both mines by increasing the bench height to burden (BH/B) ratio. Velocity of 6.58m/s resulted with charge factor of  $0.28\text{kg/m}^3$  and velocity of 8.97m/s resulted with charge factor of  $0.41\text{kg/m}^3$  in Mine-A. In Mine-B, a velocity of 8.34m/s resulted with charge factor of  $0.18\text{kg/m}^3$  and 12.4m/s with charge factor of  $0.25\text{kg/m}^3$ . Thus in both mines A and B, the velocity of burden rock was found to increase with an increment in charge factor. Comparative results of rock mass velocity with BH/B ratio are precised in Table 2 and Table 3.

Table 2. Comparison of Velocity of rock movement with BH/B ratio

## Limestone Mine-A

Parameters	Blast number				
	1	2	3	4	5
Time (s)	1.2	1.1	0.9	0.8	0.8
Velocity (m/s)	6.58	7.68	7.95	8.29	8.97
BH/B ratio	2.0	2.4	2.8	3.0	4.0

## Limestone Mine-B

Parameters	Blast number				
	1	2	3	4	5
Time (s)	0.9	0.8	0.8	0.7	0.7
Velocity (m/s)	8.34	9.26	8.76	9.57	12.4
BH/B ratio	1.0	1.75	1.67	3.2	3.16

Table 3. Comparison of Velocity of rock movement with charge factor

## Limestone Mine-A

Parameters	Blast number				
	1	2	3	4	5
Volume ( $\text{m}^3$ )	900	1620	1800	1500	1950
Velocity (m/s)	6.58	7.68	7.95	8.29	8.97
Charge factor ( $\text{kg/m}^3$ )	0.28	0.37	0.38	0.40	0.41

Limestone Mine-B

Parameters	Blast number				
	1	2	3	4	5
Volume (m <sup>3</sup> )	360	425	450	3750	2892
Velocity (m/s)	8.34	9.26	8.76	9.57	12.4
Charge factor (kg/m <sup>3</sup> )	0.18	0.20	0.21	0.24	0.25

Output of fragmentation analysis obtained from Wipfrag based image processing analysis comprises of cumulative size in both the limestone mines and results are shown in Figures 8 and 9.

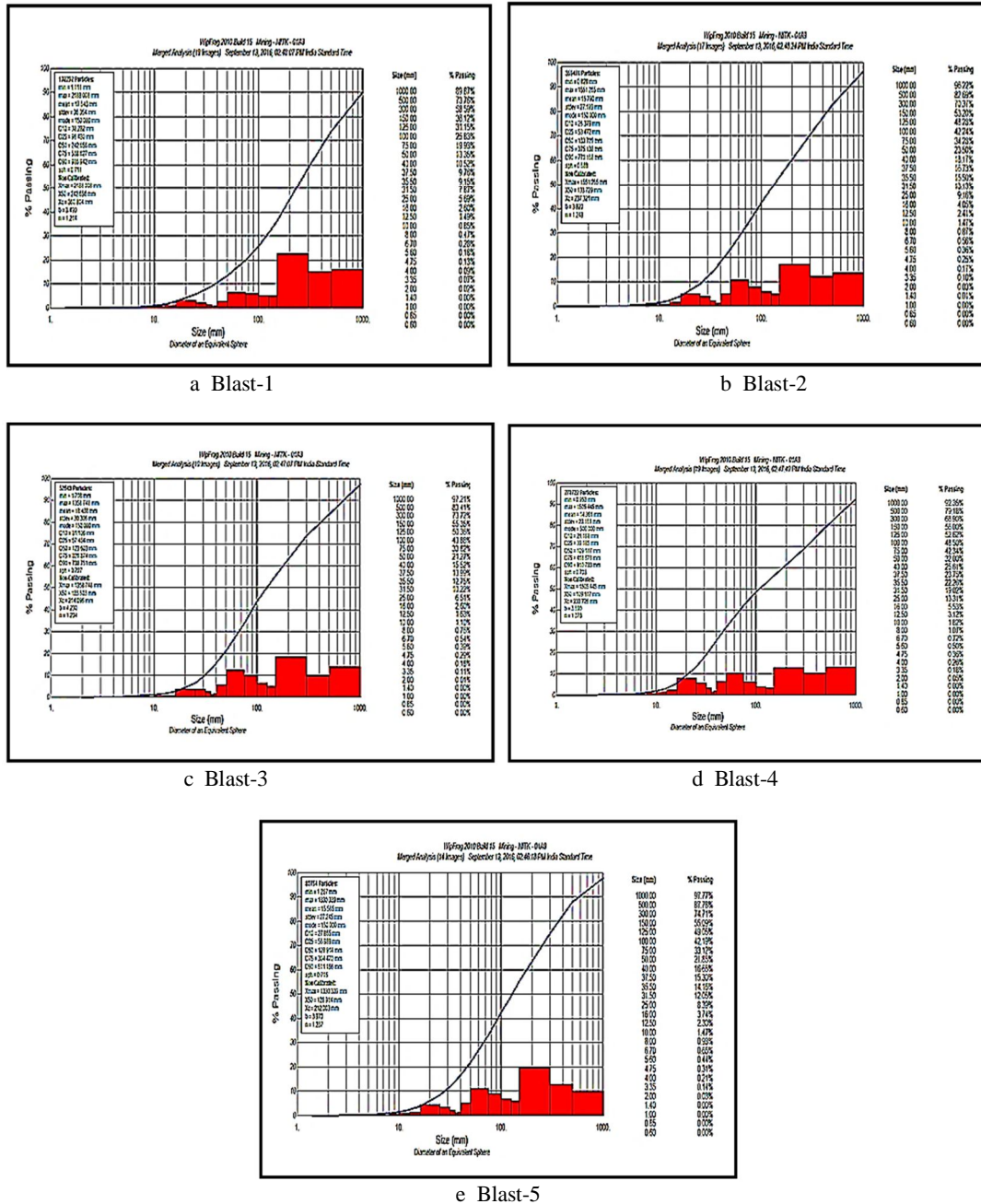


Figure 8. Fragmentation analysis of different blasts at Mine-A

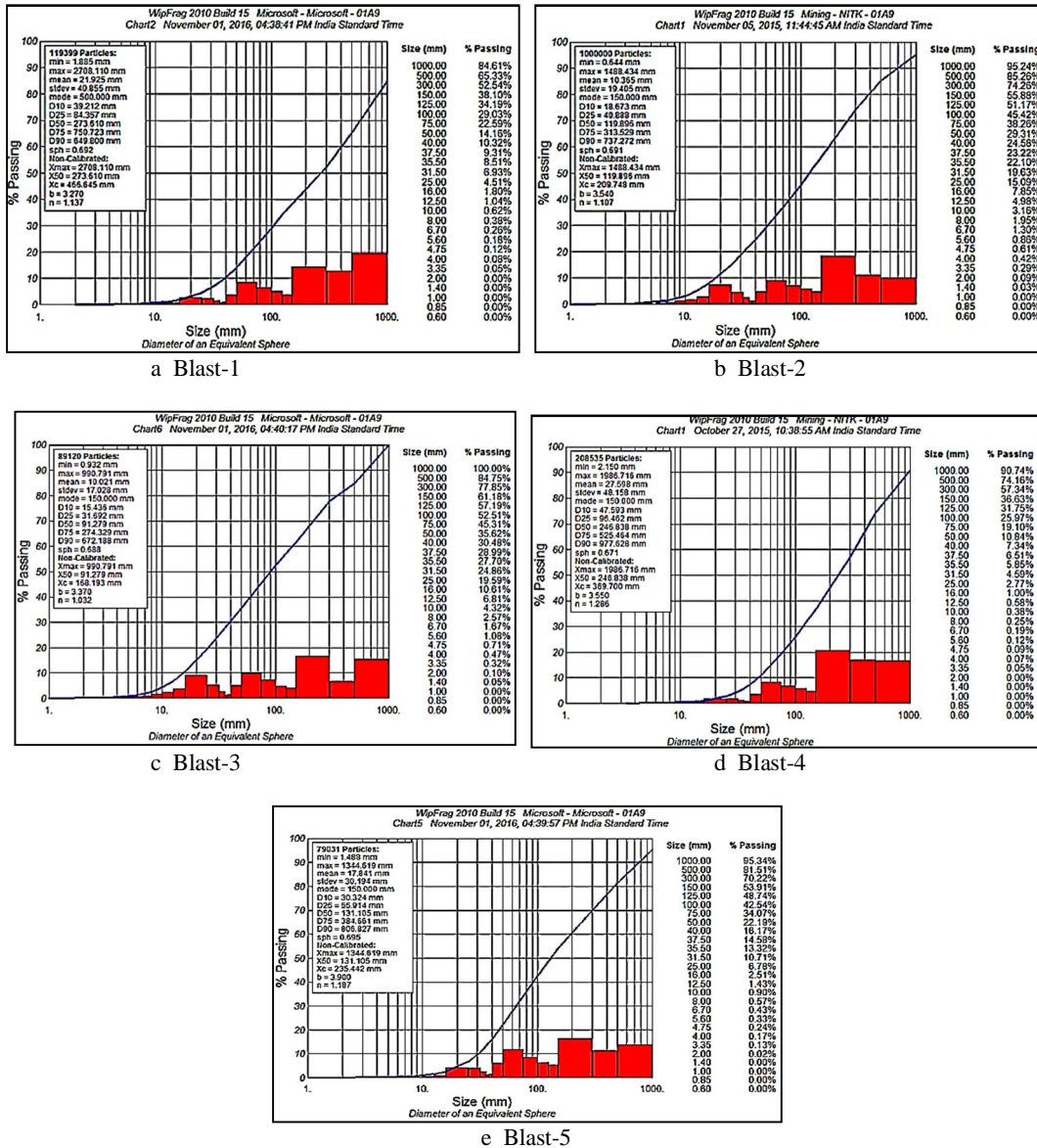


Figure 9. Fragmentation analysis of different blasts at Mine-B

Image processing based fragmentation analysis revealed major insights that may not be observed by Size naked eye. In Mine-A, Blast-4 with explosive charge of about 33.36kg/hole produced coarser fragmentation compared to Blast-5 with explosive charge of about 40.03kg/hole. In Mine-B, Blast-4 with explosive charge of about 33.33kg/hole produced coarser fragmentation compared to Blast-5 with explosive charge of about 48.21kg/hole. Similarly, in mine-A Blast-4 with explosive charge of about 33.36kg/hole produced finer fragmentation compared to Blast-4 in mine-B with explosive charge of about 33.33kg/hole. Fragmentation results of Mine-A and Mine-B are formulated in Tables 4 and 5.

Table 4. Fragmentation values obtained from blasts in Mine-A

Blast Number	Number of Holes	Percentage Passing				
		1000 (mm)	500 (mm)	300 (mm)	150 (mm)	100 (mm)
1	13	89.87	73.76	58.59	36.12	25.83
2	24	96.22	82.69	70.37	53.20	42.24
3	23	97.21	83.41	73.72	55.35	43.88
4	18	92.35	79.18	68.90	56.00	52.62
5	20	97.77	87.78	74.71	55.09	42.19

Table 5. Fragmentation values obtained from blasts in Mine-B

Blast Number	Number of Holes	Percentage Passing				
		1000(mm)	500(mm)	300(mm)	150(mm)	100(mm)
1	17	84.61	65.33	52.54	38.10	29.03
2	12	95.24	85.26	74.26	55.88	45.42
3	10	100.00	84.75	77.85	61.18	52.51
4	27	90.74	74.16	57.34	36.63	25.97
5	15	95.34	81.51	70.22	53.91	42.54

## Conclusions

High speed videography is a very good image processing tool for analysing the performance of blast in mines and quarries, in terms of tracking down the burden rock movement, behaviour of bench with different explosive loading and initiation pattern, ejection of stemming from stemming zone, role of structural discontinuities, etc. Similarly, the digital image processing techniques predicted the fragmentation size resulting from blasts quite effectively. Following are the major understandings from the study carried out in two different limestone mines:

- From the image processing analysis carried out, it was observed that bench height of 10m resulted in 7.42m of stemming ejection (on average) and bench height of 7.5m resulted in 8.73m of stemming ejection (on average). Hence, it may be concluded that increase in bench height results in lesser stemming ejection, and better utilisation of explosive energy.
- Results clearly indicating an increase in burden rock movement with upsurge in charge factor. Velocity of 6.58m/s resulted with a charge factor of 0.28kg/m<sup>3</sup>, whereas velocity of 8.97m/s resulted with increased charge factor of 0.41kg/m<sup>3</sup>. It was observed from the image processing analysis that greater velocity of rock mass movement was resulted with an increase in bench height.
- Bench height to burden (BH/B) ratio of 2.0 was resulted in burden movement / burden rock velocity of 6.58m/s and 2.8 was resulted in burden movement / burden rock velocity of 7.95m/s.
- From the Wipfrag based image processing analysis, there was a clear indication of increased charge factors resulting in enhanced fragmentation.

## Acknowledgements

Authors would like to acknowledge the management of M/s The Ramco Cements Limited and M/s Pathapadu Limestone Mine, for permitting the work. Opinions expressed in the paper are of the authors and need not be of those organizations.

## References

- [1] Ash, R.L.; (1973); The influence of geological discontinuities on rock blasting; University of Minnesota: Minnesota.
- [2] Bhandari, S.; (1997); Engineering rock blasting operations; pp. 388; Taylor & Francis: Balkema.
- [3] Chiappetta, R.F.; Mammele, M.E.; (1987); Analytical high-speed photography to evaluate air decks, stemming retention and gas confinement in presplitting, reclamation and gross motion applications; Society of Experimental Mechanics; 257–301.
- [4] Chiappetta, R.F.; Mammele, M.E.; (1988); Use Of High-Speed Motion Picture Photography In Blast Evaluation And Design; International Society for Optics and Photonics, 319–336.
- [5] CO, A.P.; (1987); Explosives and Rock Blasting; pp. 662; Atlas Powder Co: Dallas.
- [6] Floyd, J.L.; (1987); Increasing cast Blasting Benefit with the use of High Speed Motion Picture Photography and Analysis; Rock Fragmentation Blasting; 364.
- [7] Jha, A.K.; (2013); Evaluation of Mine Productivity and Economics by Effective Blast Instrumentation—A Techno Economic Proposition; Journal of Geological Resource and Engineering; **31(1)**; 31–38.
- [8] Nabiullah, M.; Jagdish, Dr.; Pingua, B.; Singh, T.; (2002); Application of high speed video technique in blasting; Journal of Mines, Metals & Fuels; **50(3)**; 54–57.
- [9] Sastry, V. R.; Venkatreddy, D.; Raghu Chandra, G.; (2014); Rock Blasting; Chap. 7, pp. 57-75; National Institute of Technology Karnataka: Mangalore.
- [10] Sastry, V.R.; Raghu Chandra, G.; Adithya, N.; Saiprasad, S.A.; (2015a); Application of High-Speed Videography in Assessing the Performance of Blasts; International Journal of Geological and Geotechnical Engineering; **1(1)**; 37–51.
- [11] Sastry, V.R.; Rajasekhar, B.; Raghu Chandra, G.; (2015b); Assessing the Explosive Energy Utilization in Mine Blasting—Role of High Speed Videography; Advanced Trends in Civil Engineering and Sustainable Development.

**B.Sc.  
Third Year**



**Sem V  
Elective**

# **Physics**

**(Solid State Physics)**



**Telugu Akademi  
Hyderabad**

Telugu Akademi Publications

B.Sc., Physics

**B.Sc.**  
**Third Year**  
**Physics**

(Semester - V)

**Solid State Physics**

(Elective)

**AUTHORS**

**Dr. M. Lakshmipathi Rao**  
Retd. Professor of Physics  
Department of Physics  
Osmania University, Hyderabad

**Dr. G. Ramadevudu**  
Senior Assistant Professor, Department of Physics  
Vasavi College of Engineering  
Hyderabad

**EDITOR**

**Dr. M. Lakshmipathi Rao**  
Retd. Professor of Physics  
Department of Physics  
Osmania University, Hyderabad



**Telugu Akademi**  
**Hyderabad**

Sem V  
Elective

**B.Sc.  
Third Year**

# Physics

(Solid State Physics)



Printed, Published & Distributed by  
**TELUGU AKADEMI**  
Himayatnagar, Hyderabad  
email : [info@teluguacademy.net](mailto:info@teluguacademy.net)  
web : [www.teluguacademy.net](http://www.teluguacademy.net)



# Structural Health Monitoring Using Admittance Response of Piezoceramic Actuator Sensors

Dr. Akshay S. K. Naidu

*Department of Civil Engineering, Methodist College of Engineering and Technology (O.U.), Hyderabad, INDIA - 500001*

akshaynaidu@methodist.edu.in

**Abstract**—This paper delineates and reviews the recent technological developments in the field of Structural Health Monitoring (SHM) using the Electromechanical Impedance (EMI) technique. The EMI technique for SHM uses piezoelectric ceramic actuator sensors that are embedded in or surface-bonded to a structural member. The changes in the electrical admittance response over an ultrasonic frequency range of the actuator sensor thus mounted indicates the changes in the dynamic structural properties, such as mass stiffness and damping. These in turn indicate the state of damage in the structure. Owing to the EMI technique's high ultrasonic frequency range of operation, this technique has the capabilities of assessing incipient damages and structural changes locally without having to know the damage location a priori. This has potential capabilities of real-time, automated, and continuous structural health monitoring.

**Keywords**—Structural Health Monitoring (SHM), Electromechanical Impedance (EMI) technique, Piezoelectric ceramic actuator sensors, Lead Zirconate Titanate (PZT), Non-destructive testing (NDT).

## I. INTRODUCTION

The economic and technological growth of a nation is reflected in the development of its infrastructure. The infrastructural development necessitates the complimentary support of the renewed maintenance, condition monitoring and retrofitting technologies. Most of the non-destructive testing (NDT) methods that are commonly adopted have a specific applicability [1], [2]. NDT methods are used for evaluation of the structural systems at the scheduled periods of inspection. These need some estimate of damage location based on expert knowledge and inferential insight of the maintenance inspector, even before testing. Further, the application of NDT methods may necessitate the portion of the structure, which needs to be inspected, to be rendered isolated and unfunctional during the duration of evaluation.

The Structural Health Monitoring (SHM) methodology aims at continuous monitoring and evaluation of the structural integrity adopting modern sensing technologies. The SHM methods do not require knowledge of the damage location a priori to the evaluation and can be applied even during the service period of the buildings, bridges or other infrastructure [3]. The electromechanical impedance (EMI) technique has come to light as a promising application for SHM [4]. The EMI technique extracts the impedance characteristics of the piezoelectric actuator/sensors that are surface bonded to or embedded into a structural member. There are many techniques using piezoelectric sensors for SHM, such as acoustic emission, ultrasonic pulse generation and more recently wave propagation techniques. This work primarily focuses on the developments made in the EMI technique for SHM.

## II. HEALTH MONITORING METHODOLOGY

### A. Piezoelectric Property

Piezoelectric materials are obtained in two forms (a) as ceramics such as the Lead Zirconate Titanate (PZT) and (b) as polymer films such as Polyvinylidene fluoride (PVDF). Their unique property renders them in to a popular class of materials, called smart materials, intelligent materials or self-adaptive materials. Piezoelectric materials deform (strain) when an electric field is applied across their polarized ends and conversely, produce voltage across their poles when subjected to mechanical strain, as shown in Figure 1. This bifunctional property makes the piezoelectrics be used both as actuators and sensors. In some applications, one PZT ceramic chip is used as an actuator and another chip in pair is used as a sensor. The actuator sensor pair is used to generate lamb waves for structural diagnosis. However, in the EMI technique, the same piezoelectric ceramic chip acts as an actuator and the sensor. Thus, the PZT ceramic chip is also referred to, in such applications, as self-sensing actuators.

# International Journal of Emerging Technology and Advanced Engineering

(E-ISSN 2250-2459, UGC Approved List of Recommended Journal, Volume 7, Special Issue 2, December 2017)

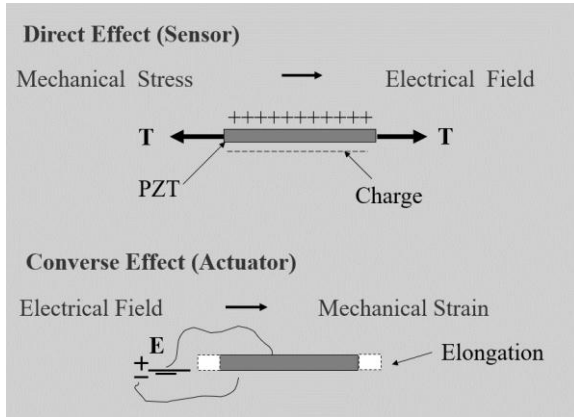


**Figure 1: PZT sensor and actuator response properties**

### B. Electromechanical Impedance (EMI) Technique

The EMI technique exploits the characteristic features of the PZT ceramic actuator/sensors by subjecting them to alternating voltage source, which induces high frequency vibration to the PZT. The PZT, which is surface-bonded onto or embedded within the structural element, induces actuation in the structure, locally. The conductance signature, that is the real part of the electrical admittance ( $Y$ ) of the PZT as a function of the excitation frequency, is extracted using impedance analyzers or LCR meters.

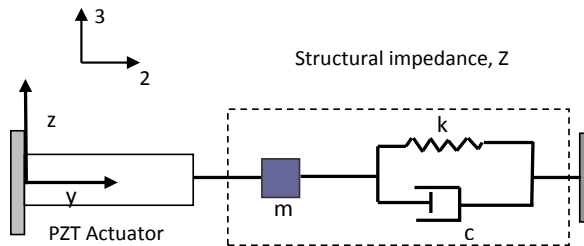


**Figure 2: SDOF system actuated by a PZT actuator**

The expression for the electrical admittance (inverse of impedance) of the PZT ceramic chip driving the host structure, modelled as a single-degree-of-freedom (SDOF) system as illustrated in Figure 2, has been derived and is available in the literature, which is expressed as [5]

$$Y = \omega j \frac{w_a l_a}{h_a} \left[ \overline{\epsilon}_{33}^T + \left( \frac{Z_a}{Z + Z_a} \right) d_{32}^2 \overline{Y}_{22}^E \left( \frac{\tan k l_a}{k l_a} \right) - d_{32}^2 \overline{Y}_{22}^E \right] \dots (1)$$

where  $w_a$ ,  $l_a$  and  $h_a$  represent the PZT width, length and thickness, respectively.  $\omega$  is the angular frequency of the applied alternating voltage,  $Z$  is the mechanical impedance of the host structure, and  $Z_a$  is the mechanical impedance of the PZT transducer,  $\overline{\epsilon}_{33}^T$  and  $d_{32}$  are piezoelectric constants and  $\overline{Y}_{22}^E$  is the complex Young's modulus.

As observed in equation (1), there exists a coupling between mechanical impedances of the PZT and the host structure, in producing the output electrical admittance. Damage in a structure alters the mass, stiffness and damping characteristics locally, which alters the mechanical impedance of the host structure. The changes in the mechanical impedance of the structure, reflects in the changes in the electrical conductance (Re  $Y$ ) of the PZT. This serves as the damage indicator. The same principle is applicable when modelling PZT-structure interaction in 2D and 3D. An example of experimentally obtained admittance signatures that get altered before and after damage occurrence is shown in figure 3 [6]. More specifically, the signatures are for conductance, the real part of the complex admittance. By signature, we mean the admittance response over a frequency range of actuation. These are similar to the frequency response functions used in the vibration analysis of structures, the only difference being the actuating frequency range.

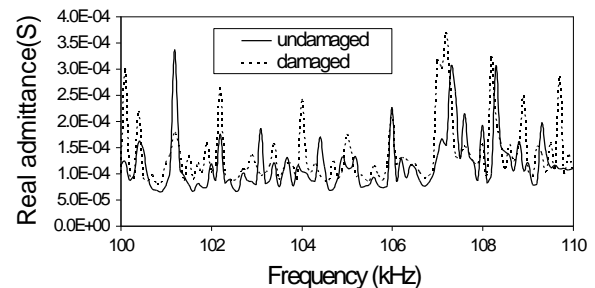


**Figure 3. Real admittance signatures for damaged and undamaged states (in siemens)**

### III. TECHNICAL ASPECTS OF THE EMI TECHNIQUE

#### A. Test Equipment Requirement

The admittance signature of the PZT actuator sensor is usually acquired using commercially available impedance analyzers, such as HP 4192A impedance analyzer, Agilent E4980A Precision LCR meter, Wayne Kerr Precision impedance analyzer [4], [7].

## International Journal of Emerging Technology and Advanced Engineering

(E-ISSN 2250-2459, UGC Approved List of Recommended Journal, Volume 7, Special Issue 2, December 2017)

An image of such equipment is shown below in Figure 4. The commonly used electrical conducting wires are used to connect the PZT actuator sensor and the impedance analyzer. One end of the two wires is soldered to the two opposite electrodes of the PZT actuator sensor. The other ends of the wires are connected to the terminals of the impedance measuring equipment.

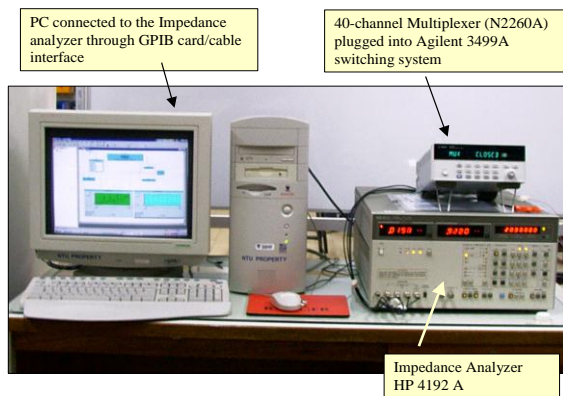


**Figure 4: Typical Impedance Measuring Equipment [6]**

### B. Power Requirement

The impedance analyzer imposes an alternating voltage signal of 1 volts rms (root mean square) to the bonded PZT actuator sensor over the user specified pre-set frequency range. It has been observed that higher excitation voltage has no influence on the conductance signature, but might only be helpful in amplifying weak structural modes [8].

### C. Influence of Adhesive

The adhesives usually used to bond the PZT actuator sensor chips on to the structure are epoxy resins. The adhesive has to transfer the high frequency mechanical actuation of the PZT to the structure. Adhesive layer must also be a transparent via medium to allow coupling of the host structure with the PZT. Thus, epoxy used must be of high shear modulus after hardening and must be of smallest possible thickness for achieving uniform bonding. The effect of the adhesive layer on the quality of admittance signatures, both real part - conductance and the imaginary part – susceptance, have been extensively studied [9].

### D. PZT Dimensions

Annamdas and Soh [10], [11] showed that the decrease in thickness for the same ‘length and width’ resulted an increase of amplitude for first major peak in admittance signature, and vice-versa. Increase in ‘length and width’ for the same thickness resulted a horizontal shift of first major peak towards left, and vice-versa.

### E. Sensing Zone

The sensing radius of a typical PZT actuator sensor might vary anywhere from 0.4 m on composite materials structures to about 2m on metallic beams [7], [12].

### F. Frequency Range of Actuation

The conductance signature of the PZT is acquired over a high frequency range in the pristine or ‘healthy’ state of the structure. Later, whenever desired to assess the structural health, the signature is extracted again and compared with the pristine signature. For effective detection of the changes in signatures appropriate frequency range may be chosen. Park and co-workers [13] recommended a frequency range from 30 kHz to 400 kHz for obtaining the admittance signatures of the PZT actuator sensors 5 to 15mm in size. A higher frequency range (>200 kHz) is favorable in localizing the sensing range, while a lower frequency range (<70 kHz) covers a large sensing area.

### G. Damage Metrics

The prominent effects of structural damages on the conductance signature are the appearance of new peaks in the signature and lateral and vertical shifting of the peaks, which are the main damage indicators. Many pattern recognition techniques to quantify these variations have been reported in the literature, such as the root mean square deviation (RMSD), waveform chain code (WCC) technique, the signature assurance criteria (SAC), the adaptive template matching (ATM), relative deviation (RD), mean absolute percent deviation (MAPD), Coefficient of correlation (CC) and Covariance (Cov) [7], [8], [12]. These are all non-parametric and purely statistical damage metrics. Naidu and Soh [14], [15] demonstrated that purely statistical damage metrics do not capture the very important effects on structural dynamic parameters, such as the natural frequency, due to structural damages. The parametric metrics try to capture changes in natural frequency and modal parameters, and give better insight in identifying location as well as the severity of the damage.

### H. Temperature Effects

The conductance signatures of the PZT actuator sensors are temperature sensitive. Thus, the effects on the signature due to damage and due to temperature exist simultaneously. This necessitates a method to decouple the two. Over a small frequency band, the overall effect of temperature has been observed to be a superposition of uniform horizontal and vertical translations of the signature [8].

## International Journal of Emerging Technology and Advanced Engineering (E-ISSN 2250-2459, UGC Approved List of Recommended Journal, Volume 7, Special Issue 2, December 2017)

This is different from the signature deviation resulting from any damages, which cause an abrupt and local variation. Thus, the effect due to temperature can be compensated with suitable corrections to the admittance signatures before going ahead for damage assessment [16].

#### IV. EMI TECHNIQUE FOR SHM APPLICATIONS

There have been numerous reports on successful proof-of-the-concept tests for damage identification in structures with the EMI technique [4], [13], [17].

The most prominent applications in localized damage identification have been reported on lab-sized truss structure, large scale prototype truss joint, steel bridge joints and pipe joints [18]–[20], RC Bridge of 5m span subjected to destructive flexural load test [21], in plain concrete structures [22], steel and aluminium plates [6] and aircraft panels and components [23], [24]. In all of these applications, it was shown that for the PZT sensor that was in a closer vicinity to the induced damage, the damage metrics estimating the changes in PZT conductance signatures were higher compared to the values for those PZTs that were far away from the location of the damage. Thus, by using an array of PZT actuator sensors in different critical locations of the structure will enable in localizing the damage occurrences for long term monitoring of structures. It has also been observed in some of the these works that the EMI conductance signatures are not affected by the mechanical noise due to random impacts or motions such as vehicular motions on bridges. This is because the operating frequency range in EMI technique is in the ultrasonic range ( $> 20$  kHz), which the mechanical noise has much lower frequencies, usually.

The EMI technique has been used along with a damage prognosis model based on linear elastic fracture mechanics concept to estimate the remaining useful life of structure subjected to fatigue [25].

The EMI technique has also been used to monitor the axial and flexural stresses in beams to distinguish them from damage induced changes in the conductance signatures [26]–[29].

The EMI technique has been applied for monitoring initial hydration of concrete [30], [31] and strength gain during curing period [32], [33]. Extending the application of the method, the EMI technique has been successfully tested as a potential method for corrosion assessment of RC structures, which is a critical factor for its durability. Previous works on corrosion detection using EMI have also been reported in the work [34].

Even in the field of retrofitting and strengthening of structures, the EMI method has been applied for monitoring the debonding of CFRP laminates and FRP rebars [35], [36]. Use of embedded PZT actuator sensor as smart aggregate for concrete strength and health monitoring is also reported [37]–[40].

#### V. TECHNICAL DEVELOPMENTS OF THE EMI TECHNIQUE

##### A. Miniaturization and low-cost variants of EMI technique

Typically, the impedance measuring devices, such as HP4192A/HP4194A impedance analyzers are used for extracting the admittance signature of the surface bonded or embedded PZT actuator sensors. The data is extracted into a computer via an I/O interface software. The main disadvantage of this equipment is its bulky size and difficulty in portability from one place to another for testing. Further, the impedance analyzer along with the test fixtures for PZT for EMI may cost about US \$ 40,000 i.e. about 26 lakhs in INR. Further, the capabilities of the highly sophisticated impedance analyzers are highly under-utilized in the EMI technique. The cost of the PZT ceramic actuator sensors are in addition to the equipment, however the cost of a PZT ceramic actuator sensor piece is cheap, at around US \$ 1, i.e. about 60 INR. Alternative to Impedance Analyzers, LCR meters have also been used along with proper test fixture for extracting the admittance signature of the PZT. LCR meter is a relatively less sophisticated instrument with lesser features than the impedance analyzer. However, its cost is also in the range of US \$ 15,000 – 25,000 for a new piece, about 15 lakhs INR [17].

In an attempt to reduce the size of the equipment, Peairs and co-workers [41] developed a simplified miniature operational amplifier based turnkey device, that uses a digital signal analyzer with a FFT function (HP 35665 A). The circuit employed by Peairs and co-workers consisted of a small resistance (typically  $<10 \Omega$ ), connected in series with the PZT actuator sensor bonded to the structure to be monitored. This newly configured circuit along with the more commonly available Digital Signal Analyzer has been successfully demonstrated for structural damage identification applications. Further, the cost of this equipment is about US \$ 15,000 – 20,000 less than the impedance analyzer. Giurgiutiu and Xu [42] also developed a field-portable small-sized impedance analyzer for EMI method.

## **International Journal of Emerging Technology and Advanced Engineering** (E-ISSN 2250-2459, UGC Approved List of Recommended Journal, Volume 7, Special Issue 2, December 2017)

Panigrahi and co-workers [43] improvised on the method used by Peairs, by doing away with the FFT analyzer and instead using a function generator (Agilent 33220A) to generate the voltage signal. Agilent 54622D mixed signal oscilloscope was employed to measure the output voltage at each excitation frequency. The total cost of the equipment used was about \$5000 only.

Bhalla and co-workers [44] proposed another system with still lower cost of about USD 2000, about 1.3 lakh INR . It utilized Agilent 34411A digital multi-meter and a very basic function generator. However, the system was limited in the sense that it only provided measurement of the magnitude of admittance and not the phase.

Kaur and co-workers [45] brought in another variation to the above hardware configuration set-up. The function generator is retained to generate the voltage signal. A new feature is that NI Express Chassis is used to measure output voltage at each excitation frequency and its phase lag with respect to the input voltage. The resulting admittance function is complex, quite akin to the measurement of the impedance analyzer.

### *B. Integration with Wireless Technology*

It has been reported in the literature that the length of the wires connecting the PZT to the impedance measuring instrument can have adverse effect on the admittance signatures if the length of the wires exceeds 30 m [4]. Further, when considering mounting an array of sensors to a structure, managing all the wires becomes extremely cumbersome and confusing. Thus, researchers have made attempts to adopt wireless technology to overcome these issues.

One of the first attempts towards a wireless system for EMI was investigated by Mascarenas and co-workers [46], who developed a portable, miniaturized and a low-cost impedance measurement chip. Its application was successfully tested in detecting load changes in a bolted frame structure. The wireless communication and local signal processing at the sensor node was investigated by integrating the device with a microprocessor and telemetry.

Incorporating the principal component analysis (PCA)-based data compression and k-means clustering-based pattern recognition, Park and co-researchers [47] developed an EMI-based wireless SHM technology. The hardware system consisted of a miniaturized impedance measuring chip (AD5933) and a self-sensing macro-fiber composite (MFC) patch.

While having many advantages, the limitation was that the frequency range of interrogation was restricted to 10-100 kHz, which is much less than the frequency ranges of HP impedance Analyzers (5 Hz to 13 MHz for HP 4192A and 100 Hz to 40 MHz for HP 4194A model) or Agilent LCR (20 Hz to 2 MHz) meter.

Another such wireless active sensing system was developed by Grisso and co-researchers [48]. Overly and co-researchers at the Los Alamos National Laboratory, New Mexico, USA further developed a Wireless Impedance Device (WID 2.0) consisting of the previously used impedance measuring chip, microcontroller chip, wireless telemetry device and data storage chip all within a board of size 5.5 x 3.7 cm<sup>2</sup> [49]. This device was portable, operating at 2.8V and would take 6 seconds to measure four sensors with 100 points and four averages per point. The developments revealed good potential for the further development of the wireless technology.

Further developments of the battery powered based wireless sensor node for the EMI technique is adequately summarized by Annamdas and Radhika [17].

### *C. Energy Harvesting Units for EMI Technique*

The continuous interrogation and monitoring requirements for the EMI method for a practical implementation of large scale SHM applications requires a constant power supply. In many cases, the remote and critical locations of a structure are inaccessible on a regular basis. To connect the PZT actuator sensors to the impedance measuring devices with long wire in those remote locations induces technical inaccuracies. On the other hand, using many sets of impedance measuring devices to access the PZT actuator sensors becomes very expensive and impractical. Wireless sensor nodes seem to be a workable solution. However, the wireless adaptations are all dependent of battery power supply, which is limited and can cause interruptions and discrepancies for long-term SHM applications.

Energy harvesting technologies could supplement the power requirements of the wireless system for EMI to further enhance its capabilities for real life applications. Annamdas and Radhika [17] have summarized the various developments in the energy harvesting technologies, based on tapping either solar energy or vibration energy, with the view of possible applications in the EMI method for SHM. Few attempts have been reported in this connection.

## International Journal of Emerging Technology and Advanced Engineering

(E-ISSN 2250-2459, UGC Approved List of Recommended Journal, Volume 7, Special Issue 2, December 2017)

A low power dependent and self-powered wireless EMI-based SHM sensor node using a Texas Instruments MSP430 evaluation board was developed [50]. The sensor node performs a SHM interrogation at pre-assigned intervals, and wirelessly transmits reports to the host computer. Consuming only 0.3 J per operation, it is easily supplemented by the energy harvested from vibrations of structures. Further research and implementation studies need to be carried out for this end.

### *D. Ring dual sensor variation of EMI technique*

A new impedance measurement technique based on a dual PZT actuator sensor was developed using two separate but concentric PZT segments [51]. Because of the unique independent excitation and sensing mechanism for the segments, the dual PZT-EMI technique is shown to measure the structural responses, which are usually subdued in the conventional impedance techniques. The dual PZT impedance are shown to have the resonance peaks identical to those obtained by the conventional EMI method. The main advantage of the dual PZT technique is less vulnerability to temperature variations. The technique is particularly useful the structure being monitored is massive. This new variant technique requires further investigations for its implementation as the other conventional EMI technique.

## VI. CONCLUDING REMARKS

In this paper, the fundamental concept of the Electro-Mechanical Impedance method (EMI), the technical requirements of the method and the numerous proof-of-the-concept tests for Structural Health Monitoring (SHM) applications are briefly discussed. The EMI method utilizes the impedance characteristics of the self-sensing piezoelectric ceramic actuator/sensors (PZT) for SHM. The recent technical developments in the areas of miniaturization of the testing equipment, the cost-effective adaptations of the technique, integration with wireless technologies and the energy harvesting methods have been discussed and the futuristic developments have been highlighted. The EMI method has a potential to develop into a unique SHM system.

## REFERENCES

- [1] J. Hola and K. Schabowicz, "State-of-the-art non-destructive methods for diagnostic testing of building structures—anticipated development trends," *Arch. Civ. Mech. Eng.*, vol. 3, no. 10, pp. 5–18, 2010.
- [2] Training Course Series - Guidebook on non-destructive testing of concrete structures. 2002, International Atomic Energy Agency, Vienna.
- [3] D. Balageas, C.-P. Fritzen, and A. Güemes, *Structural health monitoring*, vol. 493. Wiley Online Library, 2006.
- [4] V. G. M. Annamdas and C. K. Soh, "Application of electromechanical impedance technique for engineering structures: review and future issues," *J. Intell. Mater. Syst. Struct.*, vol. 21, no. 1, pp. 41–59, 2010.
- [5] C. Liang, F. P. Sun, and C. A. Rogers, "An impedance method for dynamic analysis of active material systems," *J. Vib. Acoust.*, vol. 116, no. 1, pp. 120–128, 1994.
- [6] A. S. K. Naidu, "Structural damage identification with admittance signatures of smart PZT transducers," PhD Thesis, Nanyang Technological University, Singapore, 2004.
- [7] K. K. Tseng and A. S. K. Naidu, "Non-parametric damage detection and characterization using smart piezoceramic material," *Smart Mater. Struct.*, vol. 11, no. 3, p. 317, 2002.
- [8] F. P. Sun, Z. A. Chaudhry, C. A. Rogers, M. Majmundar, and C. Liang, "Automated real-time structure health monitoring via signature pattern recognition," in *Smart Structures & Materials' 95*, 1995, pp. 236–247.
- [9] S. Bhalla and S. Moharana, "A refined shear lag model for adhesively bonded piezo-impedance transducers," *J. Intell. Mater. Syst. Struct.*, vol. 24, no. 1, pp. 33–48, 2013.
- [10] V. G. M. Annamdas and C. K. Soh, "Three-dimensional electromechanical impedance model. I: Formulation of directional sum impedance," *J. Aerosp. Eng.*, vol. 20, no. 1, pp. 53–62, 2007.
- [11] V. G. M. Annamdas and C. K. Soh, "Three-dimensional electromechanical impedance model. II: Damage analysis and PZT characterization," *J. Aerosp. Eng.*, vol. 20, no. 1, pp. 63–71, 2007.
- [12] S. Bhalla, "A mechanical impedance approach for structural identification, health monitoring and non-destructive evaluation using piezo-impedance transducers," PhD Thesis, Nanyang Technological University, Singapore, 2004.
- [13] G. Park, H. Sohn, C. R. Farrar, and D. J. Inman, "Overview of piezoelectric impedance-based health monitoring and path forward," *Shock Vib. Dig.*, vol. 35, no. 6, pp. 451–464, 2003.
- [14] A. S. K. Naidu and C. K. Soh, "Identifying damage location with admittance signatures of smart piezo-transducers," *J. Intell. Mater. Syst. Struct.*, vol. 15, no. 8, pp. 627–642, 2004.
- [15] A. S. K. Naidu and C. K. Soh, "Damage severity and propagation characterization with admittance signatures of piezo transducers," *Smart Mater. Struct.*, vol. 13, no. 2, p. 393, 2004.
- [16] G. Park, K. Kabeya, H. H. Cudney, and D. J. Inman, "Impedance-based structural health monitoring for temperature varying applications," *JSME Int. J. Ser. Solid Mech. Mater. Eng.*, vol. 42, no. 2, pp. 249–258, 1999.
- [17] V. G. Annamdas and M. A. Radhika, "Electromechanical impedance of piezoelectric transducers for monitoring metallic and non-metallic structures: A review of wired, wireless and energy-harvesting methods," *J. Intell. Mater. Syst. Struct.*, vol. 24, no. 9, pp. 1021–1042, 2013.
- [18] J. W. Ayres, F. Lalonde, Z. Chaudhry, and C. A. Rogers, "Qualitative impedance-based health monitoring of civil infrastructures," *Smart Mater. Struct.*, vol. 7, no. 5, p. 599, 1998.
- [19] G. Park, H. H. Cudney, and D. J. Inman, "Impedance-based health monitoring of civil structural components," *J. Infrastruct. Syst.*, vol. 6, no. 4, pp. 153–160, 2000.

## International Journal of Emerging Technology and Advanced Engineering

(E-ISSN 2250-2459, UGC Approved List of Recommended Journal, Volume 7, Special Issue 2, December 2017)

- [20] G. Park, H. H. Cudney, and D. J. Inman, "Feasibility of using impedance-based damage assessment for pipeline structures," *Earthq. Eng. Struct. Dyn.*, vol. 30, no. 10, pp. 1463–1474, 2001.
- [21] C. Soh, K. K. H. Tseng, S. Bhalla, and A. Gupta, "Performance of smart piezoceramic patches in health monitoring of a RC bridge," *Smart Mater. Struct.*, vol. 9, no. 4, p. 533, 2000.
- [22] A. S. Naidu and S. Bhalla, "Damage detection in concrete structures with smart piezoceramic transducers," in *Smart Materials, Structures, and Systems*, 2003, pp. 684–690.
- [23] V. Giurgiutiu and A. Zagrai, "Damage detection in simulated aging-aircraft panels using the electro-mechanical impedance technique," *ASME-Publ.-AD*, vol. 60, pp. 349–358, 2000.
- [24] V. Giurgiutiu, A. Zagrai, and J. Bao, "Embedded Active Sensors for In-situ Structural Health Monitoring of Aging Aircraft Structures," *Proc. 7th ASME NDE Top. Conf.*, vol. 20, 2001.
- [25] Y. Y. Lim and C. K. Soh, "Fatigue life estimation of a 1D aluminum beam under mode-I loading using the electromechanical impedance technique," *Smart Mater. Struct.*, vol. 20, no. 12, p. 125001, 2011.
- [26] M. Abe, G. Park, and D. J. Inman, "Impedance-based monitoring of stress in thin structural members," *UNIT 45002 APO AP 96337-5002*, p. 285, 2001.
- [27] C.-W. Ong, Y. Yang, A. S. Naidu, Y. Lu, and C. K. Soh, "Application of the electro-mechanical impedance method for the identification of in-situ stress in structures," in *SPIE's International Symposium on Smart Materials, Nano-, and Micro-Smart Systems*, 2002, pp. 503–514.
- [28] V. G. M. Annamdas, Y. Yang, and C. K. Soh, "Influence of loading on the electromechanical admittance of piezoceramic transducers," *Smart Mater. Struct.*, vol. 16, no. 5, p. 1888, 2007.
- [29] Y. Y. Lim and C. K. Soh, "Effect of varying axial load under fixed boundary condition on admittance signatures of electromechanical impedance technique," *J. Intell. Mater. Syst. Struct.*, p. 1045389X12437888, 2012.
- [30] Y. Yang, B. S. Divsholi, and C. K. Soh, "A reusable PZT transducer for monitoring initial hydration and structural health of concrete," *Sensors*, vol. 10, no. 5, pp. 5193–5208, 2010.
- [31] V. Talakokula, S. Bhalla, and A. Gupta, "Monitoring early hydration of reinforced concrete structures using structural parameters identified by piezo sensors via electromechanical impedance technique," *Mech. Syst. Signal Process.*, vol. 99, pp. 129–141, 2018.
- [32] S. Bhalla, A. S. Naidu, C. W. Ong, and C.-K. Soh, "Practical issues in the implementation of electro-mechanical impedance technique for NDE," in *SPIE's International Symposium on Smart Materials, Nano-, and Micro-Smart Systems*, 2002, pp. 484–494.
- [33] V. G. M. Annamdas, Y. Yang, and C. K. Soh, "Impedance based concrete monitoring using embedded PZT sensors," *Int. J. Civ. Struct. Eng.*, vol. 1, no. 3, pp. 414–424, 2010.
- [34] V. Talakokula and S. Bhalla, "Reinforcement corrosion assessment capability of surface bonded and embedded piezo sensors for reinforced concrete structures," *J. Intell. Mater. Syst. Struct.*, p. 1045389X14554133, 2014.
- [35] S. Park, J.-W. Kim, C. Lee, and S.-K. Park, "Impedance-based wireless debonding condition monitoring of CFRP laminated concrete structures," *NDT E Int.*, vol. 44, no. 2, pp. 232–238, 2011.
- [36] W. Li, S. Fan, S. C. M. Ho, J. Wu, and G. Song, "Interfacial debonding detection in fiber-reinforced polymer rebar-reinforced concrete using electro-mechanical impedance technique," *Struct. Health Monit.*, p. 1475921717703053, 2017.
- [37] G. Song, H. Gu, and Y.-L. Mo, "Smart aggregates: multi-functional sensors for concrete structures—a tutorial and a review," *Smart Mater. Struct.*, vol. 17, no. 3, p. 033001, 2008.
- [38] G. Song, H. Gu, Y. L. Mo, T. T. C. Hsu, and H. Dhonde, "Concrete structural health monitoring using embedded piezoceramic transducers," *Smart Mater. Struct.*, vol. 16, no. 4, p. 959, 2007.
- [39] S. Jain, S. S. Prakash, and K. V. L. Subramaniam, "Monitoring of Concrete Cylinders With and Without Steel Fibers Under Compression Using Piezo-Ceramic Smart Aggregates," *J. Nondestruct. Eval.*, vol. 35, no. 4, p. 59, 2016.
- [40] A. Narayanan and K. V. Subramaniam, "Experimental evaluation of load-induced damage in concrete from distributed microcracks to localized cracking on electro-mechanical impedance response of bonded PZT," *Constr. Build. Mater.*, vol. 105, pp. 536–544, 2016.
- [41] D. M. Peairs, G. Park, and D. J. Inman, "Improving accessibility of the impedance-based structural health monitoring method," *J. Intell. Mater. Syst. Struct.*, vol. 15, no. 2, pp. 129–139, 2004.
- [42] V. Giurgiutiu and B. Xu, "Development of a field-portable small-size impedance analyzer for structural health monitoring using the electromechanical impedance technique," *SPIE's 11th Annu. Int. Symp. Smart Struct. Mater. 9th Annu. Int. Symp. NDE Health Monit. Diagn.*, pp. 14–18, 2004.
- [43] R. Panigrahi, S. Bhalla, and A. Gupta, "A Low-Cost Variant of Electro-Mechanical Impedance (EMI) Technique for Structural Health Monitoring," *Exp. Tech.*, vol. 34, no. 2, pp. 25–29, 2010.
- [44] S. Bhalla, A. Gupta, S. Bansal, and T. Garg, "Ultra low-cost adaptations of electro-mechanical impedance technique for structural health monitoring," *J. Intell. Mater. Syst. Struct.*, 2009.
- [45] N. Kaur, L. Li, S. Bhalla, and Y. Xia, "A low-cost version of electro-mechanical impedance technique for damage detection in reinforced concrete structures using multiple piezo configurations," *Adv. Struct. Eng.*, vol. 20, no. 8, pp. 1247–1254, 2017.
- [46] D. L. Mascarenas, M. D. Todd, G. Park, and C. R. Farrar, "Development of an impedance-based wireless sensor node for structural health monitoring," *Smart Mater. Struct.*, vol. 16, no. 6, p. 2137, 2007.
- [47] S. Park, J.-J. Lee, C.-B. Yun, and D. J. Inman, "Electro-mechanical impedance-based wireless structural health monitoring using PCA-data compression and k-means clustering algorithms," *J. Intell. Mater. Syst. Struct.*, vol. 19, no. 4, pp. 509–520, 2008.
- [48] B. L. Grisso, L. A. Martin, and D. J. Inman, "A wireless active sensing system for impedance-based structural health monitoring," in *Proc. of 23rd Inter. Modal Anal. Conf.(IMAC XXIII)*. Orlando, FL, 2005.
- [49] T. G. Overly, G. Park, K. M. Farinholt, and C. R. Farrar, "Development of an extremely compact impedance-based wireless sensing device," *Smart Mater. Struct.*, vol. 17, no. 6, p. 065011, 2008.
- [50] D. Zhou, N. Kong, D. S. Ha, and D. J. Inman, "A self-powered wireless sensor node for structural health monitoring," in *Proc. SPIE Int. Soc. Opt. Eng.*, 2010, vol. 7650, p. 765010.
- [51] H. Song, H. J. Lim, and H. Sohn, "Electromechanical impedance measurement from large structures using a dual piezoelectric transducer," *J. Sound Vib.*, vol. 332, no. 25, pp. 6580–6595, 2013.

## Study on Mechanical Properties of Binary Blended Recycled Aggregate Concrete Using Rice Husk Ash

Shaista Begum<sup>1</sup>, D. Rupesh Kumar<sup>2</sup>, Sidra Khan<sup>3</sup>

<sup>1</sup>Associate Professor, <sup>3</sup>M.E Scholar, Civil Engineering, Deccan College of Engineering and Technology, Darussalam, Hyderabad, 500001, TS, India.

<sup>2</sup>Associate Professor, Civil Engineering, College of Engineering, Osmania University, Hyderabad, TS, India.

<sup>1</sup>ershaistaw@gmail.com, <sup>2</sup>rkdhondy@gmail.com, <sup>3</sup>sidrah9225@gmail.com

**Abstract**—The present experimental investigation is conducted to study the mechanical properties of binary blended recycled aggregate concrete using rice husk ash having a particle size of about 45 $\mu$  replaced with ordinary Portland cement. The experiment was conducted in three stages. In the first stage the properties such as compressive strength, split tensile strength and workability of the natural coarse aggregate were found. In the second stage properties of partially (5%,10%,15%,20%,25%,30%) and 100% replaced NCA with RCA were determined and found to be 30% less than conventional concrete at 100% replacement. This reduction was due to excess water absorption by RCA and weak interfacial Transition zone which results in lower workability. In the last stage with the aim to overcome above deficiencies of RAC with 100% RCA, Rice Husk Ash was used as the partial replacement of OPC (5%, 10%, 15%, 20%, and 25%) along with super plasticizer of about 0.8% of weight of binding material. The fresh and harden concrete properties were analyzed after 28 days of curing and found that at 10% replacement of OPC with RHA along with super plasticizer was optimum and gave compressive strength of 40.0 N/mm<sup>2</sup> which is very near to the strength of conventional concrete i.e., 39N/mm<sup>2</sup>. Similarly the split tensile strength of BBRAC mixes was found to be nearly equal to NAC. The workability of BBRAC mix with 100% RCA was found to be 53% more compare to NAC mix after addition of super plasticizer.

**Keywords**—Recycled aggregate, Ricehuskash, Binary blended, Natural aggregate, Super Plasticizer.

### I. INTRODUCTION

One of the feasible alternative is to reuse construction and demolition waste as aggregates called recycled aggregate to make new concrete called recycled aggregate concrete (RAC). The main problem preventing a broader application of RAC is the poor quality of RAC comparing to the conventional concrete. This inferiority is due to the coating of old cement mortar to the recycled aggregate. Approximately 20% of cement mortar is attached to 20mm to 30mm size aggregate particles as per the investigations made by Building Contractors Society of Japan [1].

Specific gravity of recycled aggregate was found to be 4.5% to 7.6% less when compared with specific gravity of natural aggregate as per the investigations carried by Hansen and Narud [2] and Fathei Ramdan [3] in their investigation. As per the studies of Bhikshma, V. Kishore, R.[4] and Sherif Yehia, Kareem Helal and Anaam Abusharkh[5], the rough and porous surface texture leads to excess water absorption by recycled aggregate thus leading to higher water cement ratio. Less W/C ratio and addition of super plasticizer can improve the ITZ of recycled aggregate concrete. Treatment of the recycled aggregate concrete by impregnation of silica fume solution and by ultrasonic cleaning results in the good bonding between the new cement matrix and the recycled aggregate [6]. Recycled Aggregate concrete can be an economic and useful in construction. In this present study the attempts have been made to regain the strength of Recycled Aggregate Concrete by using mineral and chemical admixtures. The rice husk ash formed under the controlled burning temperature of about 500°C to 700°C having a particle size of about 45 $\mu$  is replaced with ordinary Portland cement to enhance the packing/density of the mix because of its extreme fineness. Chemical admixture i.e., super plasticizer of about 0.8% of weight of binding material is used you improve its workability. Grading, Specific gravity test and water absorption tests are conducted on fine aggregate and recycled

Aggregates. Los Angeles test is also performed to find recycled aggregate's resistance to abrasion. Compression tests, Split tensile strength tests and workability tests are conducted [7, 8].

### II. EXPERIMENTAL INVESTIGATIONS

The following materials are used for the casting of specimens.

**Cement:** Ordinary Portland cement of 53 Grade from Ultra Tech conforming to I.S: 12269([9]) is used.

## International Journal of Emerging Technology and Advanced Engineering (E-ISSN 2250-2459, UGC Approved List of Recommended Journal, Volume 7, Special Issue 2, December 2017)

*Fine Aggregate:* River sand locally available is used conforming to I.S: 383[10].

*Recycled coarse aggregate:* The RCA of 20mm maximum size of angular shape obtained from local demolished structure in Hyderabad is used.

*Water:* Locally available portable water was used for mixing and curing which is portable and free from injurious substances that may be deleterious to concrete or steel.

*Rice husk ash:* Rice husk ash used in the present investigation is collected from the brick kiln located at the outskirts of Hyderabad which was under controlled burning of around 600-700°C and the particle of RHA is below 45 micron and specific gravity is 2.3.

*Super plasticizer:* A high range water reducing Polycarboxylate based super plasticizer (sodium naphthalene formaldehyde) supplied by BASF with relative density 1.10 was used.

### III. METHODOLOGY

The properties of cement such as normal consistency, specific gravity, fineness etc., and the properties of fine aggregates, natural coarse and recycled coarse aggregates like specific gravity, grain size, and water absorption are determined using the suitable test procedures. The details of the M30 grade Concrete mix used are tabulated in Table I is arrived at as per IS: 10262[11]. Workability test on concrete with different water-cement ratio is carried out. Concrete cubes of size 150 x 150 x 150 mm are casted in standard as per obtained mix proportions for determining the compressive strength and cylinders of diameter 150mm and height 300mm for cylindrical specimen casted for determining the split tensile strength, cured and tested following standard procedures.

### IV. DISCUSSION OF RESULTS

The tabulated results of compressive strength, split tensile strength and workability of binary blended recycled aggregate concrete specimens with 5%, 10%, 15%, 20%, 25%, 30% and 100% RCA replaced with natural aggregate and specimens with 5%, 10%, 15%, 20%, 25% RHA replaced with OPC are shown in figures 1 to 7.

In the first stage it can be clearly noticed (Figure 1 & Figure 2) that as the percentage replacement of natural coarse aggregate with RCA in the concrete increase, the compressive strength is decreasing.

Compressive strength of concrete with 100% recycled aggregate is found as 28 N/mm<sup>2</sup> and split tensile strength is found to be 3.68 N/mm<sup>2</sup>. This is because the residual cement paste on surface of recycled coarse aggregate absorbs the water and make the concrete less workable and the another reason of this is weak interfacial transition zone between the surface of coarse aggregate and new cement paste which eventually decreases the compressive strength and split tensile strength of concrete.

In the second stage in the same 100% recycled aggregate concrete, OPC is replaced with RHA in different percentages. From figure 3 it is seen that there is an increase in the compressive strength up to 10% replacement of OPC with RHA after that the replacement didn't show any positive results. This might be because rice husk ash particles will have greater surface area, the surface of Rice husk ash particle absorbs the available free water and make the concrete less workable and hence the reduction in compressive strength was noticed beyond 10% replacement of OPC with RHA.

The split tensile strength decreased from 3.85 N/mm<sup>2</sup> to 2.88 N/mm<sup>2</sup> on replacing the natural aggregate with 100% recycled aggregate (Figure 2). This is because the residual cement paste on surface of recycled coarse aggregate absorbs the water and make the concrete less workable and the another reason of this is weak interfacial transition zone between the surface of coarse aggregate and new cement paste which eventually decreases the split tensile strength of concrete.

When OPC was replaced with RHA in different percentages, it is observed in figure 4 that there is an increase in the split tensile strength up to 10% replacement of OPC with RHA after that the replacement didn't show any positive results because of greater surface area of rice husk ash particles. Rice husk ash particle absorbs the available free water and make the concrete less workable and hence the reduction in split tensile strength was noticed beyond 10% replacement of OPC with RHA.

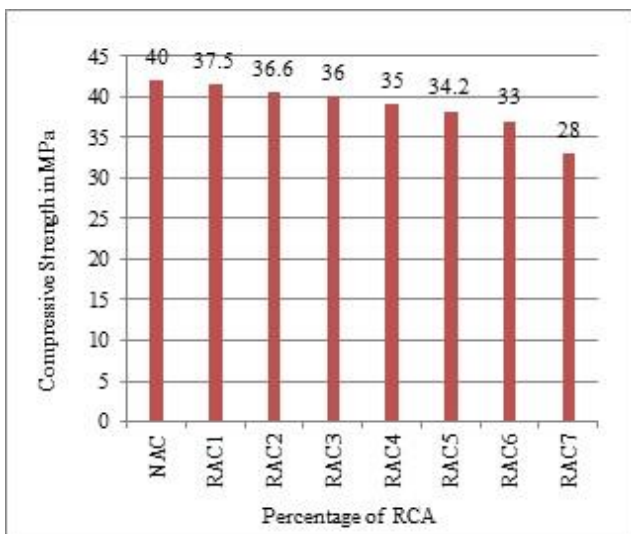
The workability which was the major concern of recycled aggregate concrete for a fixed water cement ratio is found to be maximum (Figure 5) for binary blended recycled aggregate concrete with 10% rice husk ash and 0.8% by weight of cement.

The details of the M30 Concrete mix used are given in TABLE I is arrived at as per I.S: 10262[11].

**TABLE I**  
**QUANTITY OF MATERIALS FOR GRADE M30**

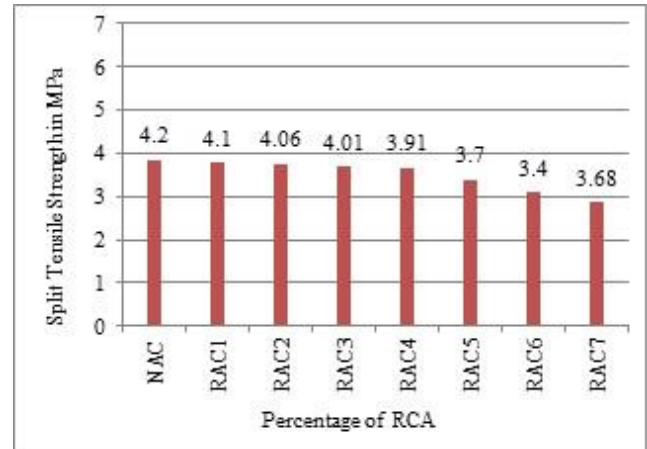
S.No.	Material (kg/m <sup>3</sup> )	Quality of material in (kg)
1.	Cement	350
2.	Rice Husk Ash	0
3.	Water	158
4.	Fine Aggregate	850
5.	Coarse Aggregate	1130
6.	Super Plasticizer	0.8% by weight of cement
7.	Water Cement Ratio (W/C)	0.45
9.	Workability	75-100 mm

Cement: Fine aggregate: Coarse aggregate is 1:2.42:3.21 with water-cement ratio 0.42.



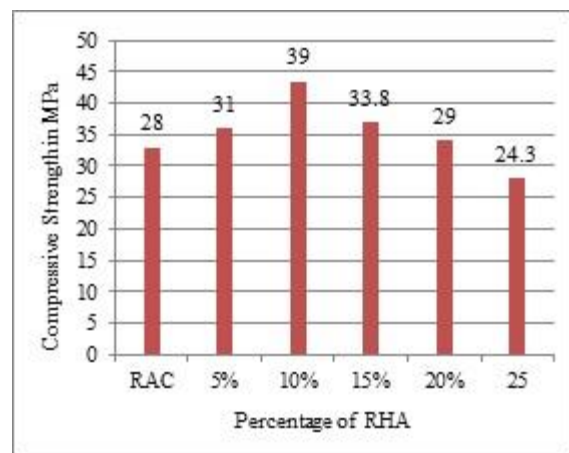
**Figure 1** Variation of Compressive Strength With Respect To Percentage Replacement of NCA with RCA

Figure 1 shows that the compressive strength of M30 grade recycled aggregate concrete is reduced with the increase in the percentage of replacement of recycled aggregate. On 100% replacement of natural aggregate, the compressive strength is reduced by 30.0%.



**Figure 2:** Variation of Split Tensile Strength with Respect to Percentage Replacement of NCA with RCA

Figure 2 shows that the split tensile strength of M30 grade recycled aggregate concrete is decreased with the increase in the percentage of replacement of recycled aggregate. On 100% replacement of natural aggregate, split tensile strength is reduced by 12.38%.

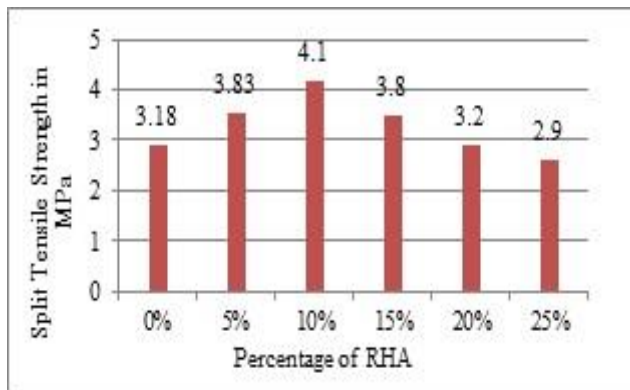


**Figure 3** Variation of Compressive Strength with Respect to Percentage Replacement to OPC with RHA

## International Journal of Emerging Technology and Advanced Engineering

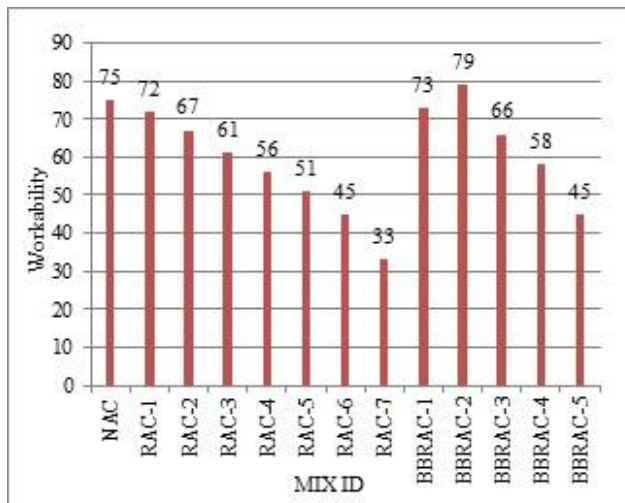
(E-ISSN 2250-2459, UGC Approved List of Recommended Journal, Volume 7, Special Issue 2, December 2017)

Figure 3 shows the increase in the compressive strength of 100% recycled aggregate concrete. The increase is 39.28% on replacement of 10% OPC with rice husk ash.



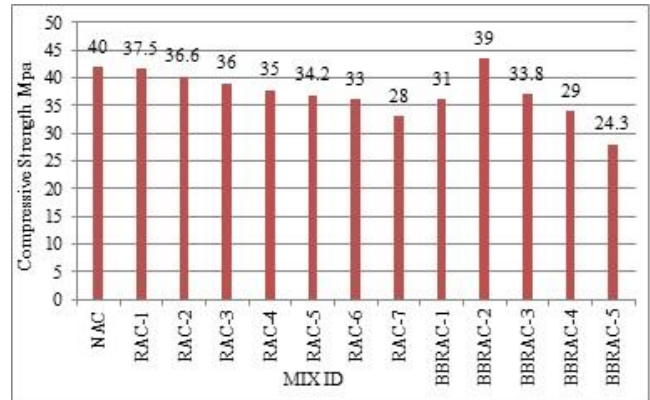
**Figure 4 Variation of Split Tensile Strength With Respect To Percentage Replacement of OPC with RHA.**

Figure 4 shows that the split tensile strength of 100% recycled aggregate concrete is increased by 38.36% on replacement of 10% OPC with rice husk ash.



**Figure 5 Variation of Workability in OPCC, RAC, BBRAC in terms Of Slump**

In Figure 5 it can be observed that by adding super plasticizer equal to 0.8% of weight of cement, the workability of recycled aggregate concrete of M30 grade is increased by 139.0%.



**Figure 6 Variation of Compressive Strength in OPCC, RAC and BBRAC**

Figure 6 shows that BBRAC-2 concrete with 100% recycled aggregate, 10% rice husk ash replaced with OPC and a suitable amount of super plasticizer has increased the compressive strength of RAC. Only a small difference of 2.50% is found between RAC and NAC.

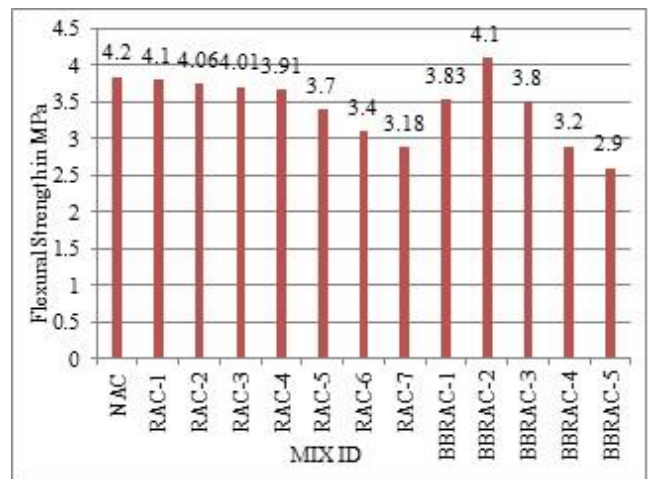


**Figure 7 Variation of Split Tensile Strength in OPCC, RAC, and BBRAC**

Figure 7 shows that BBRAC-2 concrete with 100% recycled aggregate, 10% rice husk ash replaced with OPC and a suitable amount of super plasticizer has increased the split tensile strength and it is only 2.38% less compared to NAC.

## **International Journal of Emerging Technology and Advanced Engineering** (E-ISSN 2250-2459, UGC Approved List of Recommended Journal, Volume 7, Special Issue 2, December 2017)

### V. CONCLUSIONS

1. The compressive strength and split tensile strength of 100% replaced M30 grade RAC is found to be 30% and 12.38% less when compared to M30 grade conventional mix.
2. The compressive strength and split tensile strength of binary blended recycled aggregate concrete (BBRAC) mix was found to be 39.28% and 38.36% more when compared to RAC with 100% recycled aggregate.
3. The workability of BBRAC was found to increase by 139% after addition of super plasticizer when compared to RAC with 100% recycled aggregate.

### *Acknowledgements*

The authors wish to thank the managements and the academic teaching and non-teaching faculties of Deccan college of Engineering and Technology, Darussalam, Hyderabad for the help provided in the completion of this project.

### REFERENCES

- [1] Study on Recycled Aggregate and Recycled Aggregate Concrete, Building Contractors Society of Japan. Committee on Disposal and Reuse of Concrete Construction Waste, Summary in Concrete Journal, Japan, No.7, 16(1978) 18-31 (in Japanese).
- [2] Hansen TC, Narud H. Strength of recycled concrete made from crushed concrete coarse aggregate, Concrete International, No. 1, 5(1983) 79-83.
- [3] Fathei Ramdan.Mochamed Solikin.Ir.srisuarjono."Effect of Recycled Coarse Aggregate on Concrete Properties", International Journal of Innovative Research in Science, Engineering and Technology, ISSN Online (2319-8753).
- [4] Bhikshma, V. Kishore, R. 2010. "Development of stress-strain curves for Recycled Aggregate Concrete", Asian Journal of Civil Engineering, Vol. 11, No. 2, pp. 253-261.
- [5] Sherif Yehia. Kareem Helal. Anaam Abusharkh.Amani Zaher. "Strength and Durability Evaluation of Recycled Aggregate Concrete", International Journal of Concrete Structures and Materials, Vol.9, issue2, pp.219-239.
- [6] Amnon Katz. "Treatments for the Improvement of Recycled Aggregate", Journal of materials in Civil Engineering, Vol.16, issue6, 2004.
- [7] I.S. 6461 (Part 7) 1973 'Mixing, laying, compaction, curing and other construction aspects'. BIS, New Delhi.
- [8] I.S. 516-1959 'Methods of test for strength of concrete' BIS, New Delhi.
- [9] I.S. 12269-1987, 'Specification for 53 grade ordinary Portland cement'. BIS, New Delhi.
- [10] I.S. 383-1970, 'Specification for coarse and fine aggregate from natural sources for concrete'. BIS, New Delhi.
- [11] I.S. 10262-2009, 'Recommended guidelines for concrete mix design'. BIS, New Delhi.



**1<sup>ST</sup> INTERNATIONAL CONFERENCE ON  
COMPUTATIONAL INTELLIGENCE & INFORMATICS  
(ICCII - 2016)**

 Springer



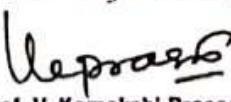
Organized by  
**Department of Computer Science and Engineering**  
JNTUH College of Engineering Hyderabad  
May 28-30, 2016

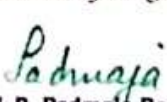
**Certificate**

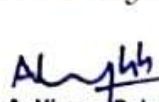
This is to certify that ..... K. Shailaja ..... of  
Methodist College of Engineering & Technology, Hyderabad  
has presented a paper entitled Progressive Genetic Evolutions based Jain Cost Optimization  
(CPGE-TCO) for Distributed RDF Chain Queries Co-Authored by Dr. P.V. Kumar, Dr. S. Durga  
Bhavani

in the 1<sup>st</sup> International Conference on Computational Intelligence & Informatics (ICCII-2016), held during May 28-30, 2016.  
This paper has been published in the proceedings of ICCII-2016, Springer-Advances in Intelligent Systems and Computing.

  
**Dr. S. C. Satapathy**  
Corresponding Editor  
Springer AISC-ICCII 2016

  
**Prof. V. Kamakshi Prasad**  
Organizing Chair  
Springer AISC-ICCII 2016

  
**Prof. B. Padmaja Rani**  
Organizing Chair  
Springer AISC-ICCII 2016

  
**Prof. A. Vinaya Babu**  
Conference Chair  
Springer AISC-ICCII 2016

  
**Prof. A. Govardhan**  
Principal  
JNTUHCEH

# *Performance Comparison of IST and Multi Scale Principal Component Analysis in the EEG Signal Processing*

Dr.B.Krishna Kumar<sup>1</sup> and Dr.K.V.S.V.R.Prasad<sup>2</sup>

<sup>1</sup>Professor, Dept.of ECE, Methodist College of Engineering and Technology, Hyderabad, TS, INDIA  
e-mail: saisantu2004@yahoo.co.in

<sup>2</sup> Prof & Head Dept. of ECE, D.M.S.S.V.H Engg.College, Machilipatnam, Andhra Pradesh  
e-mail: kvsvr@yahoo.com

## ABSTRACT

The removal of Ocular Artifacts (OA) in Electroencephalogram (EEG) data is one of the key challenges in the analysis of brain recordings. Brain activity produces electroencephalogram signals, which consists of some of vital signs of neurological disorders such as epilepsy, tumor cerebrovascular lesions and the problems associated with the trauma. These signals can be acquired by placing the electrodes on the scalp at specified positions and exists in order of 1-5 $\mu$ v, whose frequency range is DC-64 Hz. Acquisition of these signals mainly suffers from different unwanted signals (artifacts or noise) resulting in less signal information for identification.

In this paper, two algorithms are proposed namely, Multi Scale Principal Component Analysis (MSPCA) and Iterative Soft Thresholding (IST) using wavelets in removing the Ocular Artifacts (OA) present in the EEG signals. This paper discusses not only the performance comparison of two algorithms on statistical parameters of EEG signals such as Signal to Noise Ratio, (SNR), SNRI or Noise Figure (NF) and Absolute Average Error (AAE) but also estimated the run time of each algorithm i.e., computational time of each algorithm.

**Keywords:** EEG, EOG, Wavelets, Denoising, Thresholding, PCA, Multi scale PCA(MSPCA), Ocular artifacts and Wavelet transform, Iterative Soft Thresholding

## 1. INTRODUCTION

Electrooculography (EOG) artifacts inevitably and frequently interfere with the electroencephalogram (EEG) signals. Eye-movement and eye-blink artifacts are the main sources of ocular artifacts. The frequency components of EEG signals are in the order of 1-5 $\mu$ V, and their frequency content differs among the different neurological rhythms, such as, alpha, beta, delta and theta rhythms [1-4]. However,

artifacts are the outstanding enemies of high quality EEG signals. These artifacts basically fall into two major categories: technical and physiological artifacts. The technical artifacts are often found in power line noise 50/60Hz results from poor electrode application on the scalp and transducer's artifacts. The physiological artifacts are often due to ocular, heart and muscular activity; are the EOG, ECG and EMG artifacts respectively [5].

To date, many methods were presented to remove EOG artifacts. Some methods were based on regression in the time domain or frequency domain [6-8] for removing eye blink artifacts. However, they always need a reliable reference channel. Moreover, EOG Reference channel often contains brain signals which will be also removed inevitably from the EEG by the procedure of regression. Therefore, the methods based on regression may not be the best way to remove EOG artifacts.

Principal Component Analysis is among the most popular methods for extracting the information from the data and has found applications in a wide range of disciplines [9]. PCA was introduced by Pearson in 1901[10] and developed by Hotelling [11] in the year 1933. Using Multi Scale Principal Component Analysis the EEG signal is decomposed into 6 levels. Later, estimation of the statistical parameters of EEG signals is done. Finally the performance comparison of these two algorithms is made.

In this paper, IST[12] using wavelets algorithm [13] the EEG signal is decomposed into a level 4, which gives us approximate and detail coefficients. The detail coefficients which are having more noise information are processed with IST and later

estimated the statistical parameters such as SNR, SNRI and AAE [13].

The noisy EEG signal is convolved with a low and high pass filter whose impulse response is determined by the wavelet chosen. The output of each filter produces the same number of samples as the original signal, so both outputs are down sampled by 2 resulting in the Approximate and detail coefficients each with half the number of points as that of the original signal.

The coefficients represent a correlation between the signal of interest and wavelet chosen at different scales and during translation. Because all of the coefficients are preserved, the original signal or any level of decomposition can be reconstructed using a filter scheme similar to decomposition shown in Figure 1. The process is reversed and now the coefficients are up sampled (interpolated), filtered, and summed.

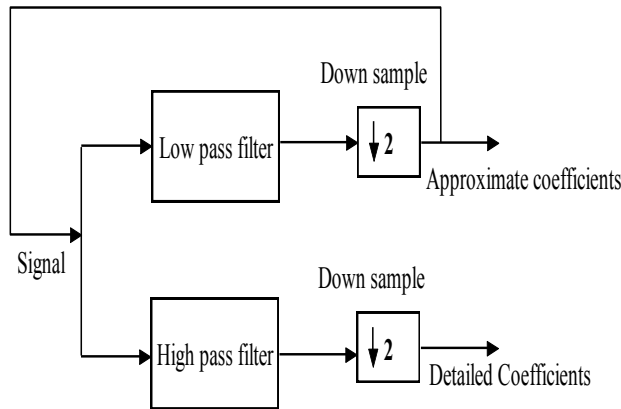


Figure.1. Block diagram to show DWT decomposition

The EEG signal is decomposed into 4 levels using dB10, Sym8 and Haar wavelets and corresponding approximate and detail coefficients are shown in the Fig.2. From derived coefficients high frequency components will be distributed in approximate coefficients and low frequency components presents in Detail coefficients cD4, cD3, cD2, cD.

## 2. ITERATIVE SOFT THRESHOLDING

This method describes an approach for the restoration of degraded signals using sparsity. This approach, which has become quite popular, is useful for numerous problems in signal processing: denoising, de convolution, interpolation, super-resolution, de

clipping, etc [12]. The observed signal  $y$  can be written as

$$y = Hx + n$$

Where  $x$  is the signal of interest which one would like to estimate,  $n$  is additive noise, and  $H$  is a matrix representing the observation processes. For example, if one observes a blurred version of  $x$  then  $H$  will be a convolution matrix. The estimation of  $x$  from  $y$  can be viewed as a linear inverse problem. A standard approach to solve linear inverse problems is to define a suitable objective function  $J(x)$  and to find the signal  $x$  minimizing  $J(x)$ [12]

Generally, the chosen objective function [12] is the sum of two terms:

$$J(x) = D(y, Hx) + \lambda R(x)$$

Where  $D(y, Hx)$  measures the discrepancy between  $y$  and  $x$  and  $R(x)$  is a regularization term (or penalty function). The parameter  $\lambda$  is called the regularization parameter and is used to adjust the trade-o between the two terms;  $\lambda$  should be a positive value. On one hand, we want to find a signal  $x$  so that  $Hx$  is very similar to  $y$ ; that is, one would like to find a signal  $x$  which is consistent with the observed data  $y$ . For  $D(y, Hx)$ , we will use the mean square error, namely

$$D(y, Hx) = \|y - Hx\|_2^2$$

The  $\|v\|_2^2$  represents the sum of squares vector ' $v$ '

### 2.1 Iterative Threshold Algorithm

The objective function minimization, previous case

$$J(x) = \|y - Hx\|_2^2 + \lambda \|x\|_1$$

The  $J(x)$  can be minimized by combining Majorization-Minimization approach

To find a majorizer of  $J(x)$ , coincides  $J(x)$  at  $x_k$  and which is easily minimized. Adding non-negative function to  $J(x)$

$$G_k(x) = J(x) + (x - x_k)^t (\alpha I - H^t H)(x - x_k)$$

By design  $G_k(x)$  coincides  $J(x)$  at  $x_k$ . one needs to minimize  $G_k(x)$  to get  $x_{k+1}$ .

From the above equation, we can get

$$G_k(\mathbf{x}) = \|\mathbf{y} - \mathbf{H}\mathbf{x}\|_2^2 + (\mathbf{x} - \mathbf{x}_k)^t (\alpha \mathbf{I} - \mathbf{H}^t \mathbf{H}) (\mathbf{x} - \mathbf{x}_k)$$

Rewriting the equation using soft thresholding,

$$G_k(\mathbf{x}) = \alpha \left\| \mathbf{x}_k + \frac{1}{\alpha} \mathbf{H}^t (\mathbf{y} - \mathbf{H}\mathbf{x}_k) - \mathbf{x} \right\|_2^2 + \lambda \|\mathbf{x}\|_1 + K$$

Where, K is constant w.r.t x. Minimizing  $G_k(x)$ , equivalent to Minimizing  $(1/\alpha)G_k(x)$  so  $x_{k+1}$ , obtained by minimizing:

$$\left\| \mathbf{x}_k + \frac{1}{\alpha} \mathbf{H}^t (\mathbf{y} - \mathbf{H}\mathbf{x}_k) - \mathbf{x} \right\|_2^2 + \frac{\lambda}{\alpha} \|\mathbf{x}\|_1$$

Therefore minimizing is achieved by the following soft-thresholding equation [12]

$$\mathbf{x}_{k+1} = \text{soft} \left( \mathbf{x}_k + \frac{1}{\alpha} \mathbf{H}^t (\mathbf{y} - \mathbf{H}\mathbf{x}_k) - \mathbf{x}, \frac{\lambda}{2\alpha} \right)$$

Where  $\alpha \geq \text{maxeig}(\mathbf{H}^t \mathbf{H})$ . This gives the Iterated Soft Threshold Algorithm.

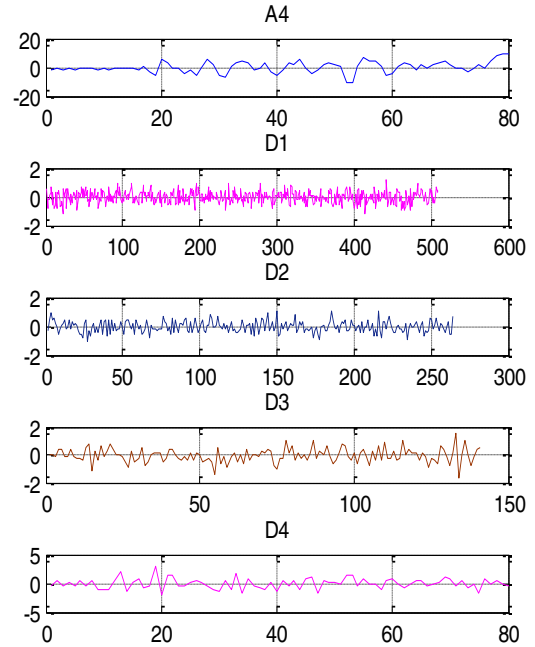
The iterative soft Thresholding algorithm is used for denoising the EEG signal. The model consists of three main steps i.e, normalization, wavelet decomposition and applying the IST for the detail coefficients. In this paper EEG signals are taken from Physionet database [15].

Data can be normalized to increase the accuracy of the application as follow:

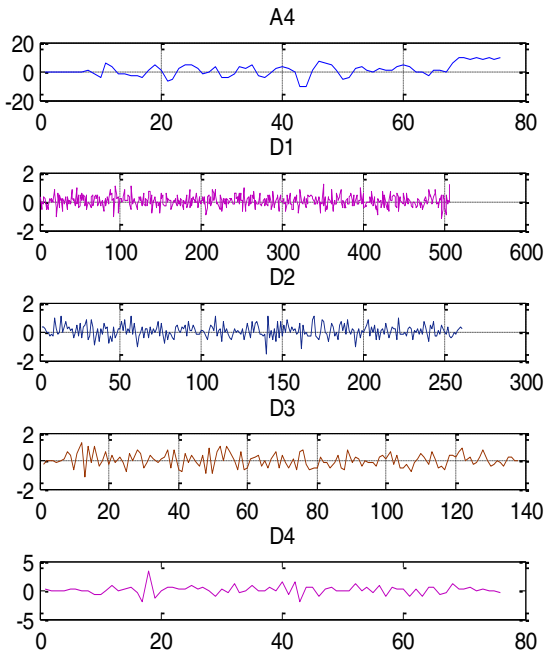
$$\mathbf{X}_{\text{norm}} = \frac{\mathbf{X} - \bar{\mathbf{X}}}{\text{std}(\mathbf{X})}$$

Normalizing of EEG signal is very important because of possible variations in signal acquisition from trial to trial, hence the normalization of data is necessary for valid results. EEG data is decomposed into 4 levels using dB10, Sym8 and Haar wavelets as shown in Figure 2(a,b and c) and all the detail coefficients are scaled by IST algorithm[13], finally by applying inverse wavelet transform results the enhanced EEG signal. Algorithmic flow result is shown in Figure 3

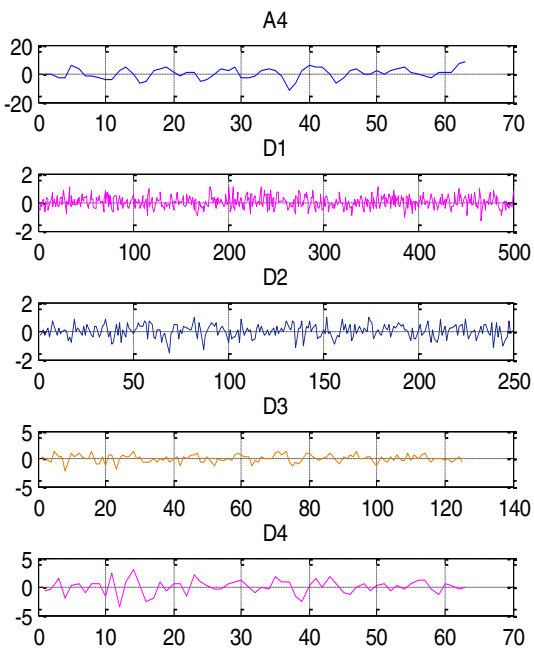
reveals that the presented method of modeling gives the good performance among all the previous techniques.



a) Approximate and detail coefficients using dB10



b) Approximate and detail coefficients using sym8



c) Approximate and detail coefficients using Haar

FIGURE 2

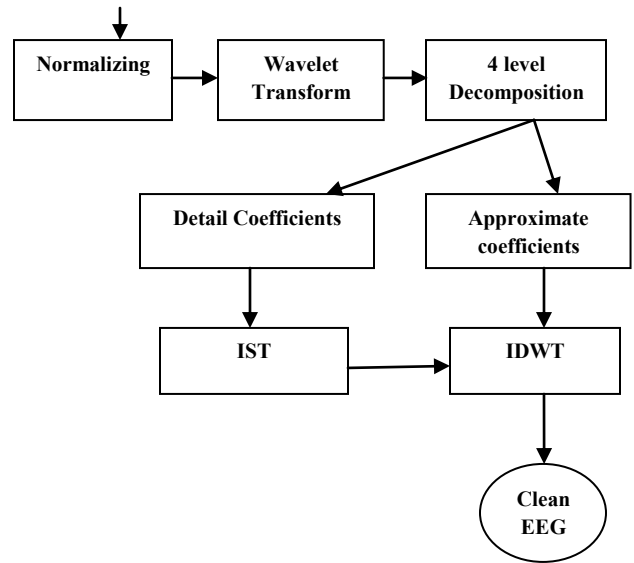


FIGURE 3: IST Using Wavelets Algorithm Flow

The noisy EEG signal and modeled EEG signal using IST algorithm is shown in the Figure 4.

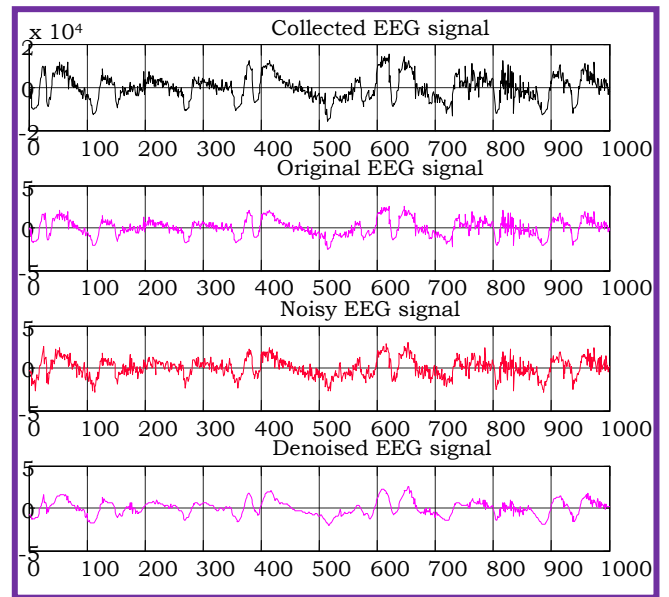


Figure.4: Noisy EEG Signal and Modeled signal

### 3. RESULTS OF IST

The results obtained from IST using wavelets algorithm [13] are provided in the Table.1

Table.1. statistical measures of EEG signal using IST

### 4. MULTISCALE PCA

PCA is a technique which is generally used for reducing the dimensionality of multivariate datasets i.e. reducing the number of dimensions, without much loss of information. Considering a vector of  $n$  random variables  $x$  for which the covariance matrix is  $\Sigma$ , the principal components (PCs) can be defined by  $z = Ax$  Where  $z$  is the vector of  $n$  PCs and  $A$  is the  $n$  by  $n$  orthogonal matrix with rows that are the eigenvectors of  $\Sigma$ . The Eigen values of  $\Sigma$  are proportional to the fraction of the total variance accounted for the corresponding eigenvectors, so the PCs explaining most of the variance in the original variables can be identified. If, as is usually the case, some of the original variables are correlated, a small subset of the PCs describes a large proportion of the variance of the original data.

Multi scale PCA (MSPCA)[14,16] combines the ability of PCA to extract the cross correlation or relationship between the variables, with that of orthonormal wavelets to separate deterministic features from stochastic processes and approximately de correlate the autocorrelation among the measurements. To combine the benefits of PCA and wavelets, the measurements for each variable (column) are decomposed to its wavelet coefficients using the same orthonormal wavelet for each variable. This results in transformation of the data matrix,  $X$  into a matrix,  $WX$ , where  $W$  is an  $n \times n$  orthonormal matrix representing the orthonormal wavelet transformation operator containing the filter coefficients.

MSPCA removes the artifacts like EMG and ocular artifacts. To remove the artifacts PCA is done twice on the same data by selecting only first four principal components, and the results were given in figures 5 for two different data sets taken from reference [15]. The results of MSPCA [14, 16] are provided in the Table.2.

Table.2. statistical measures of EEG signal using MSPCA

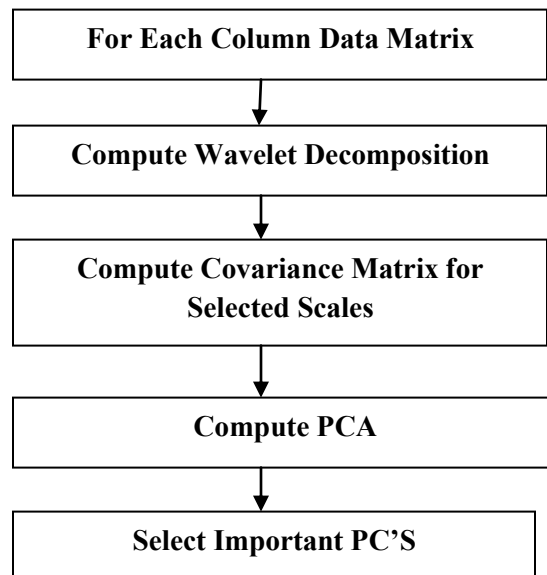
Wavelet /Threshold	AAE(dB)	SNR(dB)	SNRI(dB)
Sym8 (soft)	23.58	34.95	25.34
Sym8 (hard)	19.26	24.52	48.00
Haar (soft)	24.89	20.29	10.75

Wavelet/Thresho Id type	AAE (dB)	SNR (dB)	SNRI or NF(dB)
Sym8 (soft)	23.58	34.95	25.34
Sym8 (hard)	19.26	24.52	48.00
<b>Sym8 (IST)</b>	<b>18.26</b>	<b>38.27</b>	<b>50.20</b>
Haar (soft)	24.89	20.29	10.75
Haar (hard)	18.18	25.10	46.08
<b>Haar (IST)</b>	<b>17.22</b>	<b>39.40</b>	<b>52.30</b>
dB10(soft)	14.88	28.89	34.58
dB10(hard)	19.98	23.74	47.69
<b>dB10(IST)</b>	<b>14.44</b>	<b>29.43</b>	<b>49.43</b>
Haar (hard)	18.18	25.10	46.08
dB10 (soft)	14.88	28.89	34.58
dB10 (hard)	19.98	23.74	47.69
<b>MSPCA</b>	<b>13.72</b>	<b>37.43</b>	<b>46.91</b>

From Table.1 and Table.2 it is clearly observed that both the proposed algorithms i.e., IST and MSPCA are providing better results over the conventional Thresholding techniques namely soft and hard Thresholding.

The algorithmic flow of MSPCA [14] is shown in the Figure.5.



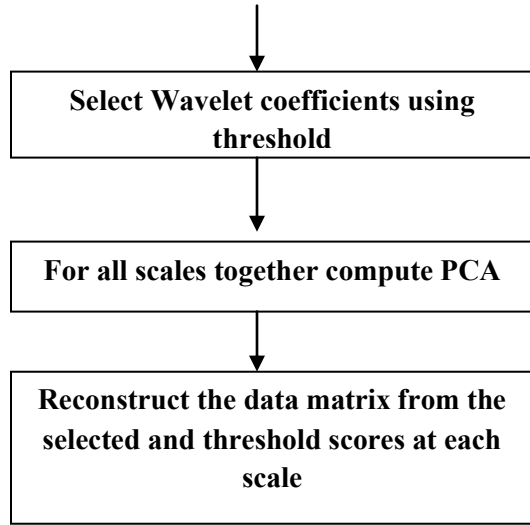


FIGURE.5: MSPCA Algorithm Flow

The noisy EEG signal and modeled EEG signal using Multi Scale Principal Component Algorithm is shown in the Figure 6.

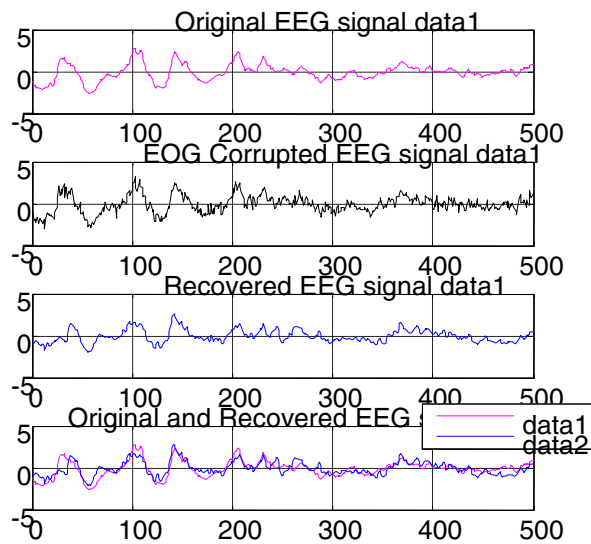


FIGURE.6: The noisy EEG signal and modeled EEG signal using MSPCA

**5. RESULTS**

Computational Efficiency of IST is better than MSPCA is provided in the Table.3. Table.3. Computational Efficiency of IST and MSPCA

Algorithm	Computational Time(sec)
IST	1.391266
MSPCA	2.694674

**6. CONCLUSIONS**

From the above Table.1, Table.2 and Table.3 it is clear that IST not only providing better statistical parameters of EEG signal but also take less time in computing them when compared to MSPCA.

**7. REFERENCES**

[1]. N.V. Thakor et al. "Multi Resolution Wavelet Analysis of Evoked Potentials", IEEE Transactions on Biomedical Engineering, Vol. 40, No 11, pp. 1085-1093, November, 1993.

[2]J.Malmivuo and R. Plonsey, "Bioelectromagnetism: Principles and Applications of Bioelectric and Biomagnetic Fields", New York: Oxford University Press, New York, Ch.28, 1995.

[3] D. Nov'ak, L. Lhotsk'a, V. Eck, and M. Sorf, "EEG and VEP Signal Processing. Cybernetics", Faculty of Electrical Engineering, pp.50-53, 2004.

[4] L. S'ormmo and P. Laguna, "Bioelectrical Signal Processing in Cardiac and Neurological Applications", Elsevier, Academic Press, 2005.

[5]. S. Ventakaramanan, P. Prabhat, S.R Choudhury, H.B Nemade, and J.S. Sahambi "Biomedical Instrumentation Based On Electrooculogram (EOG) Signal Processing And Application To A Hospital Alarm System", Indian Institute Of Technology (IIT) Guwahati, Proceedings of IEEE ICISEP, pp.535-539, 2000.

[6] Schlögl A, Keinrath C, Zimmermann D et al. "A fully automated correction method of EOG artifacts in EEG recordings" Clinical Neurophysiology.118, pp. 98-104, 2007.

[7] Jung T-P, Makeig S, Humphries C, Lee T-W, McKeown MJ, Iragui V and Sejnowski TJ. "Removing Electroencephalographic artifacts by blind source separation" Psychophysiology.37, pp.163-178, 2000.

[8] Gratton G, Coles MG and Donchin E "A new method for off-line removal of ocular artifact", Electroencephalography Clinical Neurophysiology 55(4), pp.484-486, 1983.

[9] M.Aminghafari, N. cheze, J.M Poggi, "Multivariate denoising using wavelets and principal component Analysis," computational statistics & Data Analysis, vol. 50 pp. 2381-2398, 2006.

[10] Pearson, K, "On Lines and Planes of Closest Fit to Systems of Points in Space", Phil. Magazine, vol.6, issue. 2, pp.559-572, 1901.

[11] Hotelling. H," Analysis of a Complex of Statistical Variables Into Principal Components", J. Educ. Psychol., 24, pp.417-441, pp.498-520, 1933.

[12] Ivan W.Selesnick, "Sparse Signal Restoration", pp.1-16, April6, 2010.

[13]B.Krishna Kumar, Dr.K.V.S.V.R.Prasad Dr.K.Kishan Rao and J. Sheshagiri Babu, "Modeling of EEG Signals using Wavelets with Iterative Soft Thresholding", i-

manager's Journal on Future Engineering & Technology, Vol.6, No.4, pp.37-42, May - July 2011.

[14]B.Krishna Kumar, Dr.K.V.S.V.R.Prasad, Dr.K.Kishan Rao and Narsimha Baddiri, "Analysis of EEG Signals Using Multi-Scale Principal Component Analysis", IEEE Conference, Cape Institute of Technology, Levingapuram, Kanyakumari, pp.359-363, December 15-18, 2011.

[15]<http://physionet.ph.biu.ac.il/physiobank/database>

[16] [www.mathworks.com](http://www.mathworks.com)